A Matrix Isolation Infrared and *ab-initio* Study of N-Heterocyclic Carbene and Proton Donor Solvents

Akshay Hemant Raut

A dissertation submitted for the partial fulfilment of

BS-MS dual degree in Science

Indian Institute of Science Education and Research, Mohali

April 2015

Certificate of Examination

This is to certify that the dissertation titled **"A Matrix Isolation Infrared and *ab-initio* Study of N-Heterocyclic Carbene and Proton Donor Solvents"** submitted by **Mr. Akshay Hemant Raut** (Reg. No.MS10098) for the partial fulfilment of BS-MS dual degree programme of the Institute, has been examined by the thesis committee duly appointed by the Institute. The committee finds the work done by the candidate satisfactory and recommends that the report be accepted.

Dr. P. Balanarayan Dr. Sugumar Venkataramani Prof. K S Viswanathan

(Supervisor)

Dated: April 24, 2015

Declaration

The work presented in this dissertation has been carried out by me under the guidance of Prof. K S Viswanathan at the Indian Institute of Science Education and Research Mohali.

This work has not been submitted in part or in full for a degree, a diploma, or a fellowship to any other university or institute. Whenever contributions of others are involved, every effort is made to indicate this clearly, with due acknowledgement of collaborative research and discussions. This thesis is a bonafide record of original work done by me and all sources listed within have been detailed in bibliography.

Akshay Hemant Raut

(Candidate)

Dated: April 24, 2015

In my capacity as the supervisor of the candidate's project work, I certify that the above statements by the candidate are true to the best of my knowledge.

Prof. K S Viswanathan

(Supervisor)

Acknowledgement

I would like to convey my warmest gratitude to Prof. K S Viswanathan, who gave me the opportunity to conduct my study in his research group. I wish to thank him for his guidance, generous contribution of knowledge and experience, valuable comments and encouragement from the start until the end of this project. I have really enjoyed the work under his guidance.

I am also grateful to my Master's thesis committee members Dr. Sugumar Venkataramani and Dr. P. Balanarayan for their valuable suggestions and comments during the committee meeting. My deepest gratitude also goes to Dr. R. V. Anand for his idea of appropriate precursor and for providing continuous assistance during the thesis work. I wish to thank Dr. Sanjay Singh for his help, support and permission to use different laboratory instruments. I am extremely thankful to Prof. N. Sathyamurthi, Director, IISER Mohali, for allowing me to use the various facilities of this institute to carry out research work.

I am extremely thankful to my lab members Ginny, Kanupriya, Jyoti, Pankaj, Piyush and Gargi who accompanied me throughout this research work. Thanks to Ms. Rimpi and S. Anthonysamy at IGCAR, Kalpakkam for TGA-MS analysis. I also want to thank each of my classmates who provided me a wonderful and friendly atmosphere to carry out research during the entire period.

I wish to acknowledge the Computing Facility staff for providing me excellent facilities during the computational work.

I express my sincere gratitude to each of my family members for their encouragement and moral support throughout the course of study.

Special thanks to 'Department of Science and Technology, India' for the INSPIRE fellowship, without it, my study at IISER Mohali would have not been possible.

List of Figures

List of Tables

List of Abbreviations

Abbreviation	Full form
NHC	N-Heterocyclic carbene
RHF	Restricted Hartree-Fock
DFT	Density Functional Theorem
CC	Coupled-Cluster methods
M06	Minnesota type DFT functional
MP2	Møller-Plesset second order perturbation
MP3	Møller-Plesset third order perturbation
MP4	Møller-Plesset fourth order perturbation
B3LYP	Becke-3-Parameter-Lee-Yang-Parr functional
BLYP	Becke-Lee-Yang-Parr functional
BSSE	Basis set superposition error
ZPE	Zero point energy
AIM	Atoms-in-molecules
FCC	Face centre cubic
FTIR	Fourier Transform Infrared
TGA-MS	Thermogravimetry Analysis – Mass spectrometry

CONTENTS

Abstract

Weak interactions, particularly hydrogen bonding interactions, play a crucial role in many biological and chemical systems. Most of the bio-molecular conformations are maintained by the hydrogen bonding.

Many experimental techniques have been used to study weak interactions. Matrix isolation infrared spectroscopy is one such a technique, which has proved to be efficient to study weak interactions and various conformations. The technique offers the advantage of small linewidths, which has made this technique a powerful tool to study weakly bound complexes and conformations of molecules. This technique also provides a long lifetime for reactive species and hence such species can be easily studied.

Hydrogen bonding has been extensively studied in last two decades. Very recently, hydrogen bonding interaction between carbene and proton donors such as $R_2C\cdots H\text{-}X$ has drawn considerable attention. Electron density at carbene carbon offers hydrogen bonding site. The nucleophilic nature of N-heterocyclic carbene carbon provides an opportunity to investigate hydrogen bonding interactions.

In this work, the hydrogen bonded complexes of N-heterocyclic carbene with water and methanol have been studied. Water and methanol both can act as very good proton donors. The main aim of this work is to investigate the structures of the various hydrogen bonded complexes between the precursor molecules. The computational work has been performed at R-B3LYP level of theory using 6-311++G (d, p) basis set. Two different geometries at the R-B3LYP were obtained in each case, N-heterocyclic carbene – water and N-Heterocyclic carbene – methanol. The interaction between N-heterocyclic carbene carbon and hydrogen of proton donor solvent ($NHC\cdots H\text{-}X$) has been observed as a dominating interaction in the optimized ground state. To study these complexes experimentally, the matrix isolation experimental facility has been used.

INTRODUCTION

1.1. Carbene Chemistry

1.1.1. Carbene spin multiplicity

Carbenes are neutral compounds having a divalent carbon with only six electrons in its valence shell. The reactivity of carbenes is related to their ground state spin multiplicity.[1] The geometry at the carbene carbon can be linear, described by an *sp*-hybridization of the carbene carbon, where p_x and p_y are the two degenerate nonbonding orbitals. Alternatively the structure can be bent, in which the carbene carbon acquires sp^2-hybridization. On bending, the p_y orbital remains unchanged (p_π orbital), while p_x orbital is stabilized, as it acquires some s-character (σ orbital) as shown below, where σ and p_π are the frontier orbitals.

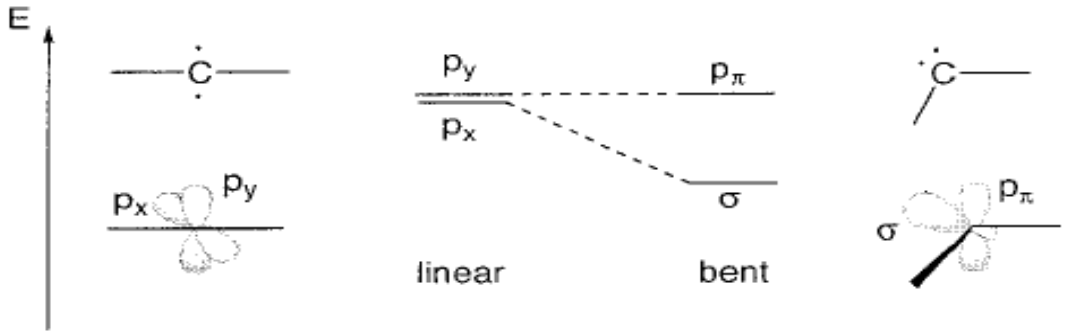

Fig. 1: Relationship between carbene bond angle and nature of frontier orbitals (from Ref. 2)

Triplet carbenes have two unpaired electrons, one in each of sp^2 and p orbital, with parallel spins and the molecule is described by $\sigma^1 p_\pi^1$ configuration. On the other hand, in singlet carbenes, two electrons are paired in a nonbonding sp^2 or p orbital. Singlet carbenes are described by σ^2 or p_π^2 configuration. Four possible electronic configurations of carbene are as shown below in **Fig.2**.

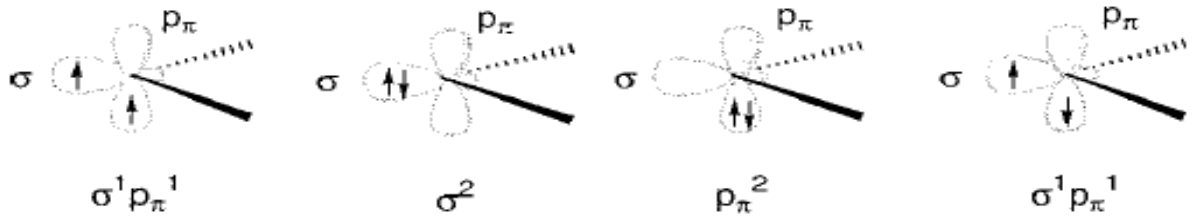

Fig.2: Electronic configurations of carbenes (from Ref. 2)

1.1.2. Influence of substituents

The ground state multiplicity of carbenes is determined by the relative energies of σ and p_π orbitals. The substituents attached to carbene carbon influence the carbene ground state multiplicity, which it can be explained in terms of inductive and mesomeric effects.

a) Inductive Effect:

Singlet state of carbene is favoured by σ-electron withdrawing substituents. When substituents are changed from electropositive lithium to electronegative fluorine, the ground state of carbene goes from a triplet to a singlet state.[3] σ-Electron withdrawing substituents induce a greater s-character, resulting in a lowering of the energy of the σ orbitals. Consequently, the σ-p_π gap increases, which favours the singlet state as shown in **Fig.3 (a)**. On the contrary, σ-electron donating substituents induce less s-character which results in a smaller σ-p_π gap, which in turn favours the triplet state **Fig.3 (b)**.

b) Mesomeric Effect:

Substituents interacting with carbene center can be classified in two classes: π-electron donating groups (X) such as -F, -Cl, -Br, -I, $-NR_2$, $-PR_2$, -OR, -SR, etc. and π-electron withdrawing groups (Z) such as –COR, -CN, $-SiR_3$, $-BR_2$, etc. When both the substituents are X, interaction of vacant p orbital with symmetric combination of substituents orbital increases the energy of the p orbital. The σ orbital remains unchanged, σ-p_π gap is increased which favours the bent singlet state as shown in **Fig.4 (a)**. When both substituents are Z, interaction of symmetric combination of substituent vacant orbitals with filled p_y orbital leads

to splitting of degenerate p_x, p_y orbitals as shown in **Fig.4 (b)**. This interaction does not affect p_x orbital. When both X and Z substituents are attached to carbene carbon, lone pair of X substituent interacts with empty p_y orbital, while vacant orbital of Z substituent interacts with p_x orbital as shown in **Fig.4 (c)** which result in quasi-linear carbenes.[2]

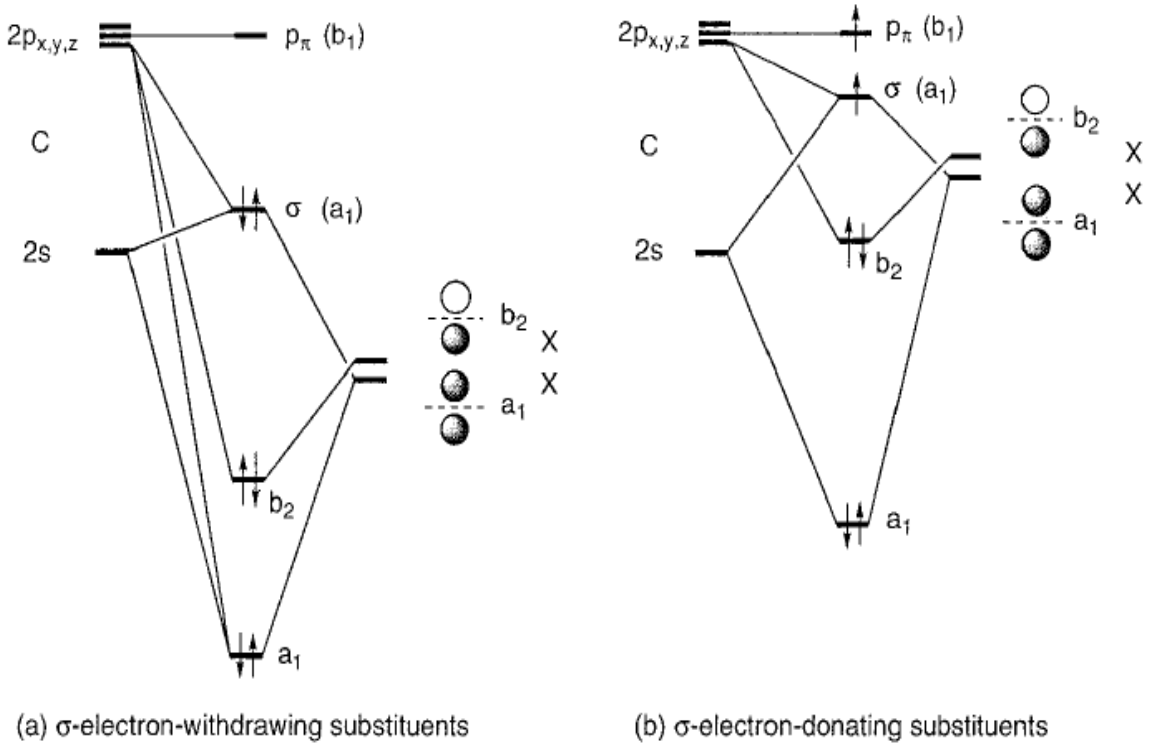

Fig.3: Molecular orbital diagram showing the influence of inductive effect (from Ref.3)

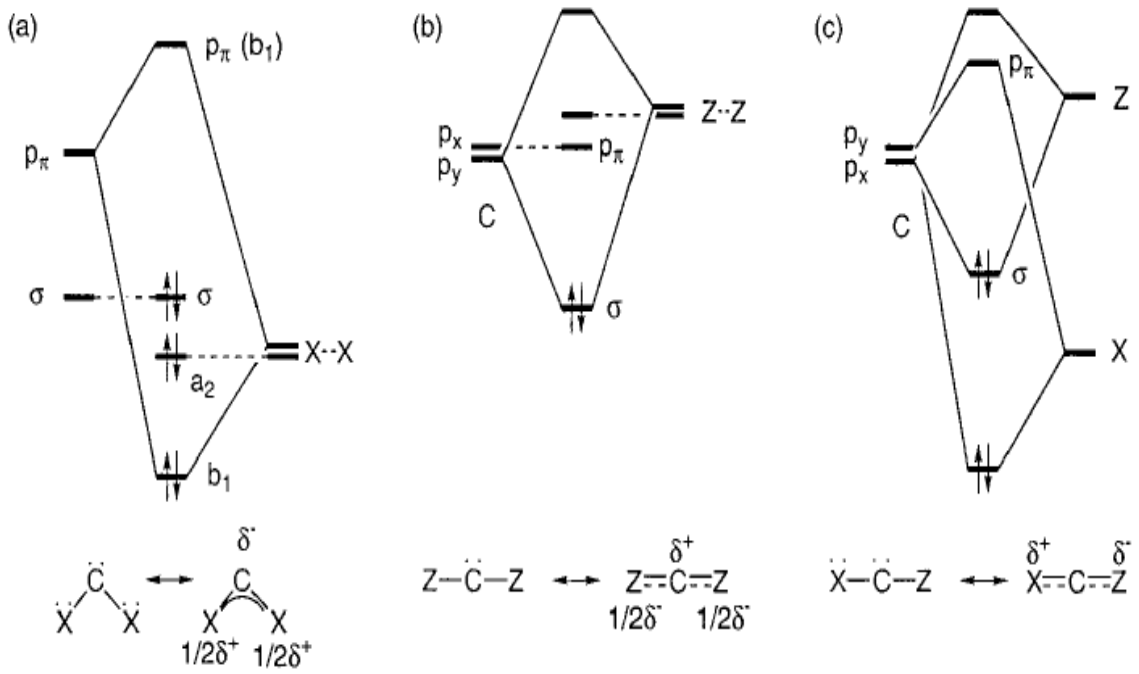

X: π-electron-donating substituents; Z: π-electron-withdrawing substituents

Fig.4: Molecular orbital diagram showing the influence of mesomeric effect (from Ref.3)

1.1.3. N-Heterocyclic carbenes

N-heterocyclic carbenes are the singlet carbenes, in which divalent carbon atom is connected directly to at least one nitrogen atom in cyclic ring. Wanzlick suggested their existence in early 1960's.[4] The first application of N-heterocyclic carbenes (NHCs) as ligands for metal complexes was reported by Wanzlick and Öfele in 1968.[5] The first stable NHC was successfully isolated by Arduengo and co-workers in 1991.[6]

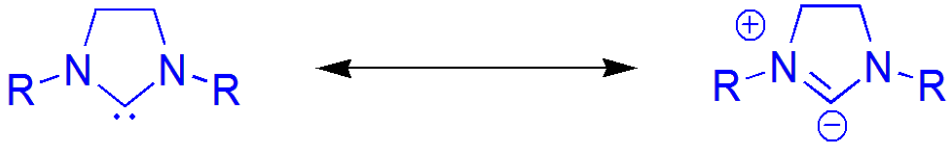

Unlike other carbenes, which are found to be ambiphilic in nature, N-heterocyclic carbenes are electron-rich nucleophilic species that are stabilized by π-electron donating and *σ*-electron withdrawing character of adjacent nitrogen centres. N-heterocyclic carbenes can

form strong bonds with metal centres than most classical ligands such as phosphines, due to their strong σ-electron donating properties and gives transition metal complexes that are generally resistant to decomposition. NHCs act as powerful ligands for stabilization of high-oxidation state metals in palladium catalyzed oxidation reactions.[7] Opppenauer-type alcohol oxidation, palladium catalyzed aerobic alcohol oxidation, Wacker-type oxidation are some of the reactions catalyzed by NHC-coordinated metal complexes.[8] Palladium catalyzed reactions, other than oxidation, include allylic alkylation[9], borylation of aryl chlorides[10], Heck reaction[11], Negishi Reaction[12], tandem coupling reactions[13]. N-heterocyclic carbenes play an important role of organocatalysts in benzoin condensation[14, 15], Stetter reaction[16, 17], etc.

1.2. Spectroscopic methods of studying carbenes

Many carbenes are relatively short lived and highly reactive in nature. However, several spectroscopic methods have been used to study these species. Time resolved absorption spectroscopy and matrix isolation spectroscopy are two techniques which have proved to be efficient to study these reactive species. Some carbenes, such as diphenylcarbene, have lifetimes of nanoseconds in solution at room temperature. Nanosecond time resolved absorption spectroscopy allows the kinetics of carbene reactions to be studied. A large number of absolute reaction rates and carbene lifetimes have been recorded that way.[18]

An entirely different approach to characterize carbenes is to immobilize these species in solid matrices at very low temperatures. A few years after the introduction of this technique by Pimentel et al.[19], Norman and Porter[20], reported reactions of methylene carbene in 1958[21] and 1959[22]. Since that time, matrix isolation spectroscopy has become a well-established technique to study these reactive species and numerous papers on the spectroscopy and reactivity of free carbenes have appeared. Many carbenes with a variety of substituents have been isolated and characterized in low temperature matrices.[23]

1.2.1. Generation of Carbenes in Matrices

Two methods mainly used for trapping the reactive species such as carbenes in matrices are 1) ***in situ* generation by photodissociation** of suitable carbene precursor (diazo or diazirines) using a laser source and 2) **vacuum pyrolysis** where carbene precursor is pyrolyzed in heated tube. Both these methods can produce well-isolated targeted species in matrices, but both have their own drawbacks.[24] Complications involved in photodissociation are as follows:

a) Photoproducts formed by photodissociation reaction can undergo bimolecular reactions such as radical – radical recombination, disproportionation, etc.
   For example, ethyl radical has been formed by photodissociation of dipropionyl peroxide isolated in Ar matrices.

$$CH_3CH_2CO_2OC\ (O)\ CH_2CH_3 + h\nu\ (\lambda > 280\ nm) \longrightarrow 2\ CH_3CH_2\cdot + 2\ CO_2$$

Since ethyl radicals are trapped in matrices, following reactions are prominent.

$$C_2H_5\cdot + C_2H_5\cdot \longrightarrow CH_3CH_2 - CH_2CH_3 \cdots\cdots \text{(Radical-radical recombination)}$$

$$C_2H_5\cdot + C_2H_5\cdot \longrightarrow CH_2CH_2 + C_2H_6 \cdots\cdots \text{(Disproportionation reaction)}$$

b) Unwanted photoproducts produce intense features in IR spectra, which lead to difficulty in identification of species of interest.

c) Close physical proximity of photoproducts lead to perturbation of IR spectra. For example, in the photodissociation of iodobenzene

$$C_6H_5I \longrightarrow C_6H_5\cdot + I\cdot$$

   C-H vibrational frequencies in phenyl radical were observed to be shifted by roughly 50 cm^{-1} due to iodine atom perturbation of its vibrational bands.

d) If the carbene precursor requires UV radiation $\lambda < 200$ nm, then atmospheric oxygen absorbs such radiation strongly. So, it is necessary to ensure that radiation leaves the lamp window within the vacuum vessel and does not travel any length in atmosphere.
   Vacuum pyrolysis method also has some drawbacks which include heat transfer to matrix, loss of reactive species by wall collisions and long residence time leading to secondary thermal reactions.

1.3. The Hydrogen bond

A hydrogen bond is an electrostatic attraction between polar molecules that occurs when a hydrogen atom is bound to highly electronegative atom such as nitrogen, oxygen or fluorine and experiences attraction to some other nearby highly electronegative atom. These hydrogen bond interactions can be intermolecular or intramolecular. The hydrogen bond is stronger than van der Waals interaction, but weaker than covalent or ionic bond. This type of bond occurs in inorganic molecules such as water and in organic molecules such as DNA and proteins.

1.3.1. Hydrogen bond studies in matrices

Matrix isolation infrared spectroscopy has proven to be very efficient technique to study hydrogen bonding interactions. A hydrogen bond leads to X-H bond lengthening with corresponding red shifts and enhanced intensity in IR spectra. In some cases, there exists weak hydrogen bond which shortens X-H bonds, showing blue shifts having decreased intensity in IR spectra. Formic acid, as the simplest carboxylic acid, is prototype for investigating hydrogen bond interactions of acids in solvent to understand microsolvation.

Sander and group have studied $HCOOH\cdots OH_2$ complexes with two hydrogen bond interactions.[25] The hydrogen bonded bromocyclohexane-ammonia complex has been isolated and characterized for the first time by Hess and Samet.[26] Two isomeric hydrogen bonded species, $N\text{-}H\cdots OH_2$ and $N\cdots H\text{-}OH$, between imidazole and water were investigated using *ab initio* calculations performed with RHF and MP2 methods.[27] Rablen et al. calculated 53 hydrogen bonded complexes of water with various small organic molecules including alcohols, thiols, esters, thioesters, carboxylic acids, esters, amines, amides, nitriles and nitro compounds, using both MP2 and B3LYP level of theory.[28]

1.3.2. Status of current research in Hydrogen bonded complexes of carbenes

Very recently, a strongly hydrogen bonded singlet ground state complex of diphenylcarbene and methanol was trapped in low temperature matrices and characterized by IR spectroscopy by Sander and Costa.[29] This hydrogen bond formation resulted in a switching of spin state of diphenylcarbene from triplet to singlet.

The labile intermediate CH_3O-H···C $(Ph)_2$ shows O-H stretching vibration due to complexed methanol at 2802 cm^{-1}, which corresponds to a large red shift of 864 cm^{-1} compared to matrix isolated uncomplexed CH_3OH. The corresponding O-D red shift in the isotopic species is 520 cm^{-1}. This proves that the complex between singlet carbene and methanol is very strongly hydrogen bonded. The singlet state is stabilized by hydrogen bonding interaction with methanol by -7.7 kcal mol^{-1} (B3LYP/6-311++G (d, p) +ZPE).[29]

Also, the first X-ray structure of N-heterocyclic carbene-alcohol hydrogen bonded complex was reported by Mohammad Movassaghi and Schmidt. The distance between carbene carbon C(2) and the oxygen of water (C···H-O) is 2.832 Å as shown in **Fig. 5**. The oxygen atom lie only 0.04 Å above the imidazolylidene ring plane and makes a nearly linear (174^0) hydrogen bond interaction.[30]

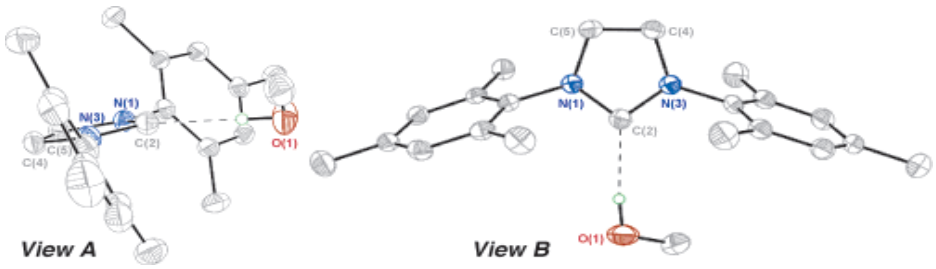

Fig.5: Alcohol-carbene H-bonded complex (from Ref. 30)

1.4. Motivation for the present work

At present, hydrogen bonding between simple carbene donor and acceptor has been studied extensively in matrix whereas hydrogen bonding of N-heterocyclic carbene in matrix still remains a challenging problem. The nucleophilic nature of NHC carbon provides opportunity to investigate hydrogen bonding interactions. It is clear from proposed mechanism **Fig. 6** and X-ray structure of N-Heterocyclic carbon-alcohol hydrogen bonded complex that electron density at C(2) of NHC offers a strong hydrogen bonding site.

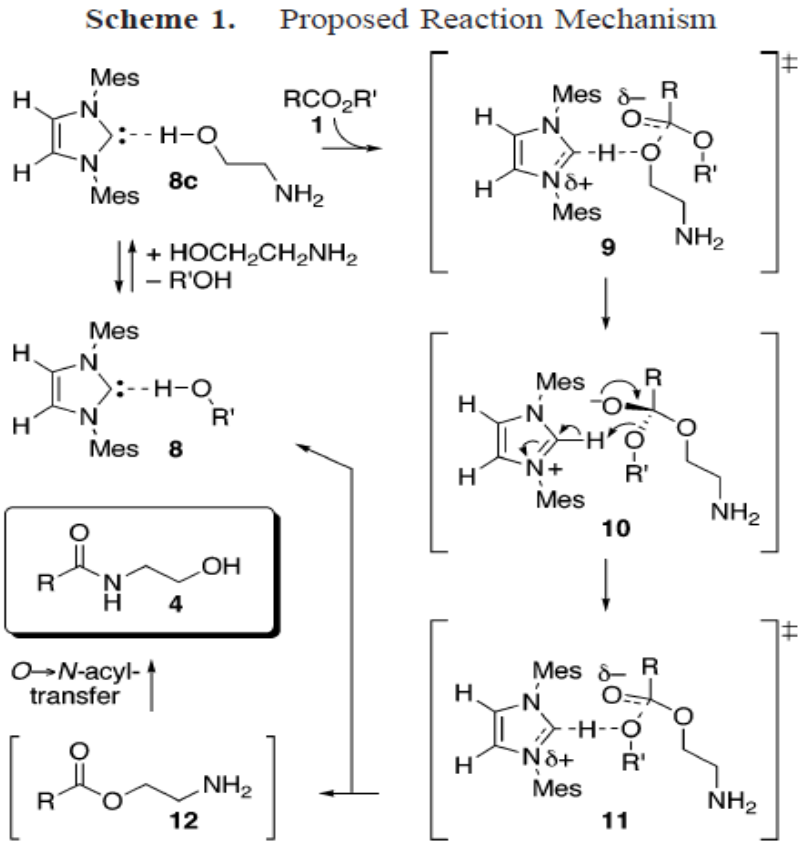

Fig.6: Proposed Pathway for transesterification (from Ref. 30)

If it can be shown that the hydrogen bonding complex of N-heterocyclic carbene with proton donor solvents can be formed, then the proposed mechanism for transesterification reaction shown above gains credence. X-ray diffraction has already provided evidence for the hydrogen bonded structure (**Fig. 5**), which our work can well corroborate.

In present study, 1, 3-dimethylimidazol-2-ylidene and proton donor solvents such as water and methanol were studied, since they provide good model systems for hydrogen bonding interactions. The active bonding sites are shown in the **Fig. 7**.

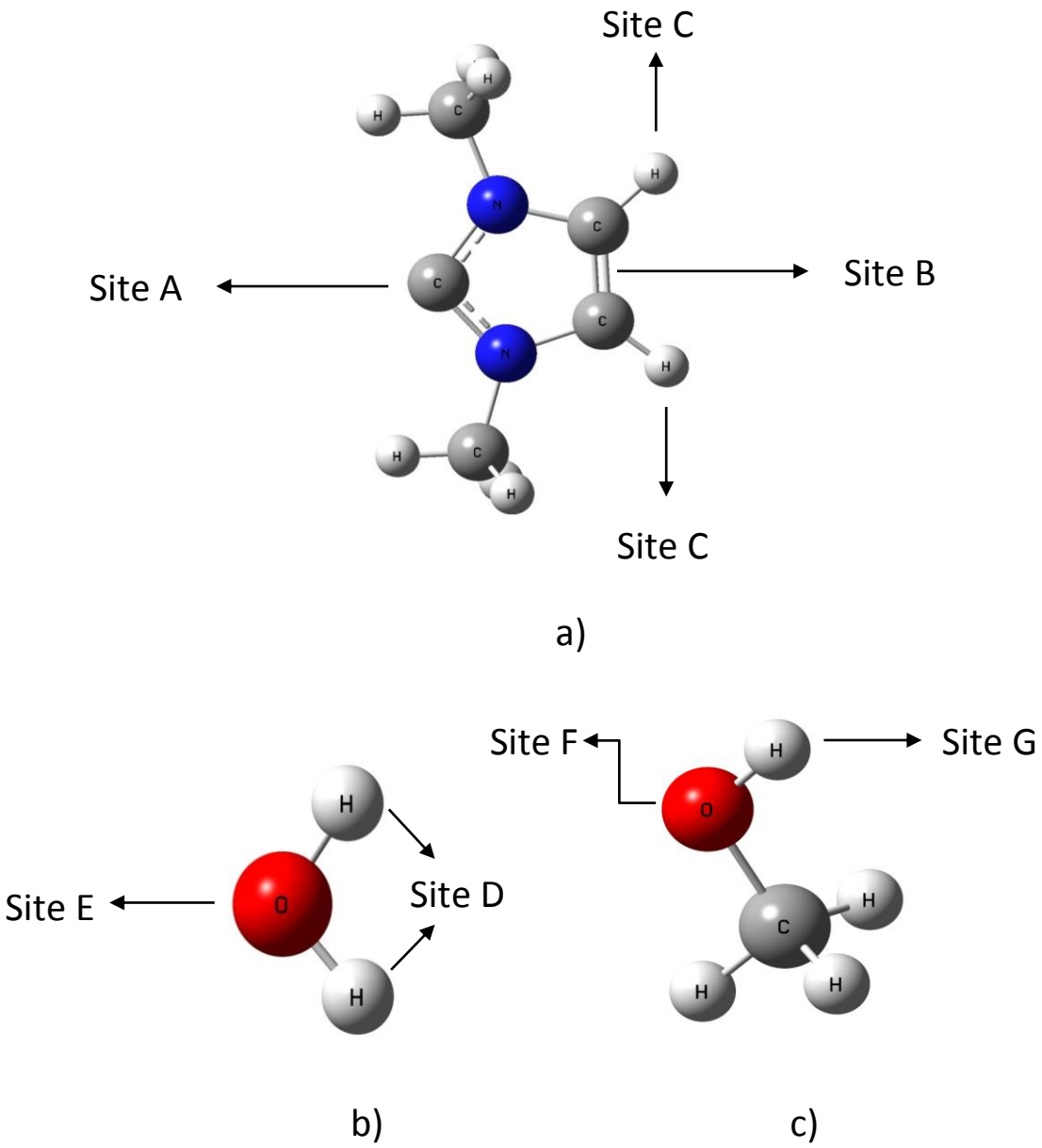

Fig. 7: Structures of a) 1, 3-dimethylimidazol-2-ylidene b) water and c) methanol indicating hydrogen bonding sites

In 1,3-dimethylimidazol-2-ylidine, both nucleophilic carbene carbon and π-cloud (Site A, Site B) can act as proton acceptor sites, whereas hydrogens of C-C double bond (Site C) can act as proton donor. In water and methanol, the hydrogens (Site D, Site G)

can act as proton donor. The oxygen of water and methanol (Site E, Site F) can act as proton acceptor. These multiple sites offered by the precursors can be expected to lead several minima.

Matrix isolation spectroscopy provides an excellent method to study the hydrogen bonded systems with multiple bonding sites as described above, as is the technique is known to trap local minima, in addition to the global minimum.

1.5. Scope and Objective of present work:

The first goal is to trap free N-Heterocyclic carbene in matrix, since free carbenes do not exist at ambient conditions due to their readily reactive nature, which may lead to dimer formation and several intramolecular rearrangements. Since, NHCs have very high boiling points and diazo precursors of NHCs are not known, a suitable precursor for its generation through a pyrolysis method needs to be identified. A carboxylate precursor 1, 3-dimethylimidazolium-2-carboxylate, was employed to obtain free carbene. TGA-MS analysis was done in order to determine the temperature at which decarboxylation takes place. The main aim is to study H-bonded interactions between N-heterocyclic carbene and proton donor solvents. The computational methods have been used to find out possible adduct between 1, 3-dimethylimidazolium-2-ylidene and proton donor solvents, water or methanol.

Chapter 2

Experimental Setup and Precursor Synthesis

The present section deals with the experimental aspects of matrix isolation infrared spectroscopy, which has been used to study the hydrogen bonded complexes of 1, 3-dimethylimidazol-2-ylidene and proton donor solvents like water and methanol. The matrix isolation technique with vacuum pyrolysis arrangement has been set up and this chapter discusses the instrumentation and synthesis aspects of experimental technique.

2.1. Matrix Isolation Technique

Matrix isolation spectroscopy is a technique where the analyte molecules are trapped in a large excess of inert gas at very low temperatures (~12 K). The typical matrices to sample ratios are from 10^3:1 to 10^5:1 in order to achieve isolation. The trapped species may be stable molecules or transient species, such as ions or radicals.

This technique was proposed and developed by George C. Pimentel and his co-workers in mid-1950, to study free radicals. Reactive species trapped in inert gas matrices have long lifetime and hence can be easily studied by various spectroscopic techniques such as infrared, UV-Visible, microwave, electron spin resonance spectroscopy. The technique offers the advantages of small linewidths, which has made this technique a powerful tool to study weakly bound complexes and conformations of molecules.

Inert gases and nitrogen are generally used in the matrix isolation technique. The matrix material should possess properties such as optical transparency in the region of interest, low volatility at the temperature of study of interest, low latent heat of fusion and acceptable thermal conductivity.

2.2. Advantages

In matrix isolation technique, the molecules do not experience intermolecular interactions since they are isolated in solid inert matrix. Doppler and collisional broadening are also absent since the molecules are immobilized in frozen matrix. The molecules are trapped at very low temperatures which ensure that only lowest electronic and vibrational levels are populated. Owing to all these reasons, the matrix isolated spectra are generally simple and sharp, unlike vapour phase and condensed phase spectra, which show usually large linewidths and spectral congestion.

2.3. Matrix environmental effects

While inert gases are chosen as matrix material, in reality the matrix is not really inert, since it usually perturbs the spectra of trapped species to a small extent due to various reasons. These matrix environmental effects are discussed below:

2.3.1. Multiple Trapping Sites

The guest species are trapped either in substitutional sites or interstitial holes in matrix. Different trapping sites will have different kind of weak intermolecular forces existing between the matrix and guest species. It is therefore possible that different trapping matrix sites may induce different shifts leading to broadening and splitting of bands. The bands corresponding to molecules trapped in stable sites, however, persist even on annealing. The bands due to splitting can be easily identified by isolating the molecule in different matrix, since two different matrices will not give rise to similar trapping sites.

2.3.2. Molecular Rotations

The molecules are tightly held and immobilized in the rigid, frozen matrix, free rotations are inhibited. Quantized rotations may be possible for small molecules such as

ammonia, water, alkali halides and methane in some matrices. The rotational features are identified by reversible intensity changes on temperature cycling, whereas splitting due to matrix side effects is not reversible on temperature cycling.

2.3.3. Aggregation

Typical matrix to analyte ratios in matrix isolation experiments are of 1000:1, at which ratios molecular isolation is reasonably assured. On increasing the solute concentration in matrix, molecules aggregate to form dimers, trimers and multimers in addition to monomers. If two species are trapped very nearby causing the overlap of their respective cages, then modification in vibrational band can be observed. The probability of intermolecular interaction to ensure the maximum isolation of analyte molecules can be calculated and it is simply chance of finding another molecule occupying one of the 12 sites that form the cage and is given by formula $P = (1-r)^{12}$, where r is the reciprocal of the matrix ratio. For very small value of r the expression becomes P = (1-12r), from this it is clear that the matrix ratio of 1000 is needed to ensure 99% isolation.

2.3.4. Matrix shifts

The solute molecules experience weak solute matrix interactions even though they are trapped in solid inert matrix under conditions of perfect isolation. These interaction can result either in a shift in the frequency or splitting of bands. The frequency shift, $\Delta\nu$ in a matrix with respect to the gas phase value arises from electrostatic ($\Delta\nu_{elec}$), inductive ($\Delta\nu_{ind}$), dispersive ($\Delta\nu_{dis}$) and repulsive interactions ($\Delta\nu_{rep}$) and is given by the following expression,

$$\Delta\nu = (\nu_{matrix} - \nu_{gas}) = \Delta\nu_{elec} + \Delta\nu_{ind} + \Delta\nu_{dis} + \Delta\nu_{rep}$$

Where, ν_{matrix} and ν_{gas} are the frequencies of the vibrational mode of a molecule in the matrix and gas phase respectively. The long range London dispersion forces and the short range repulsive forces are the two dominant interactions in inert gas matrices. The Buckingham expression[31] gives the frequency shift, $\Delta\nu$, in solutions arising from the perturbation due to solvent interactions,

$$\Delta \nu = (\nu_{solvent} - \nu_{gas}) = [B_e/hc\omega_e] [U'' - 3AU'/\omega_e)$$

where, $B_e = h/8\pi 2\mu cr_e^2$, is the rotational constant, $c\omega_e$ = harmonic oscillator frequency for the normal vibration, A =anharmonicity constant, $U' = \{\delta U/\delta r_{bc}\}$ and $U'' = \{\delta^2 U/\delta r_{bc}^2\}$

The frequency shift occurring in the matrix can be explained by the same expression. **Fig.8** shows the potential curves for a polyatomic molecule trapped in a matrix cage. There are two cases: a) When R_{CM} is greater than R_e (equilibrium distance), i.e., when one of the atoms of the trapped molecule (C) is more distant from the matrix atom (M), U' and U'' are negative and the term $\Delta \nu$ is negative. In this case, a loose cage effect is experienced by molecules which induce a negative frequency shift (red shift). b) When R_{CM} is less than R_e, U' and U'' are positive and hence $\Delta \nu$ is positive. When R_{CM} is less than R_e, the tight cage effect is experienced by molecules, which induces a positive frequency shift (blue shift).

2.4. Characteristics of Matrices

- Inertness
- Rigidity: Temperature of matrix should not exceed above one third of melting point of solid matrix
- Transparent in IR and UV-Visible region and absorption free
- Vapour pressure at room temperature should be enough for proper mixing, however at cryogenic temperature, vapour pressure should be low to form stable matrix.

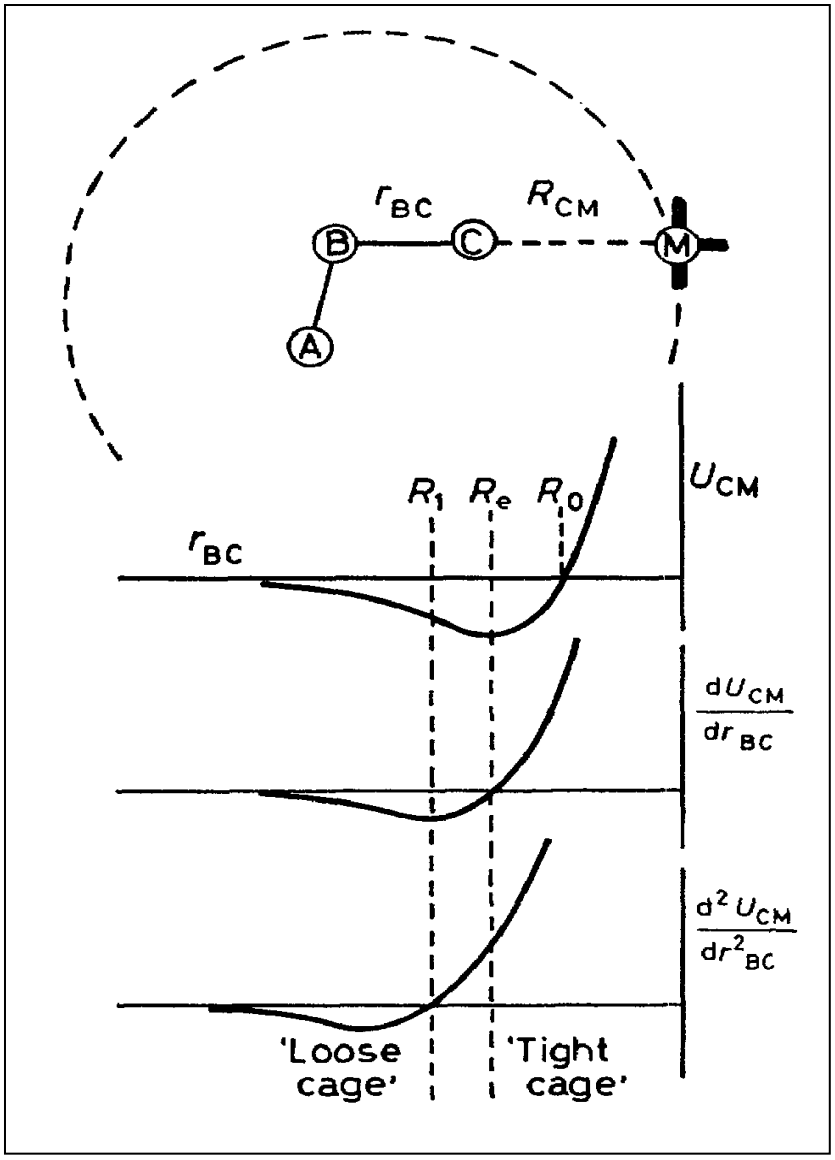

Fig. 8: Potential energy curves to show the effect of matrix cage on vibrational frequencies. (taken from Hallam, H. E. *Vibrational Spectroscopy of Trapped Species*)

2.5. Matrix structure

All the inert gases, except Helium, crystallize in face centred cubic (FCC) lattices. In FCC crystal, a species is most likely to be trapped in a substitutional site where guest molecule replaces host matrix molecule. The guest species in trapped site is surrounded by 12 nearest matrix atoms. It is not possible to accommodate the molecule of reasonable size in vacant site created by removal of one matrix atom. Hence, more than one substitutional site is generally occupied by most species. A site with 18 nearest atoms is created by removing

two matrix atoms. The substitutional sites formed by the removal of three matrix atoms in triangle will make a site with 22 nearest neighbours and loss of three matrix atoms in a row will give rise to 24 nearest neighbours.

In addition to substitutional site, crystal lattice can also have interstitial sites, Tetrahedral sites (T) and octahedral site (O). A tetrahedral site has 4 nearby matrix atoms, whereas octahedral site has 6 nearby matrix atoms. A guest molecule with a spherical diameter of 0.159 Å and 0.293 Å can be accommodated in Tetrahedral and Octahedral site respectively.

2.6. Instrumentation Setup:

The main components of matrix isolation setup involve cryostat, vacuum system and FTIR spectrometer. The photograph of matrix isolation IR spectroscopy of our lab and its main components are shown in the following **Fig. 9.**

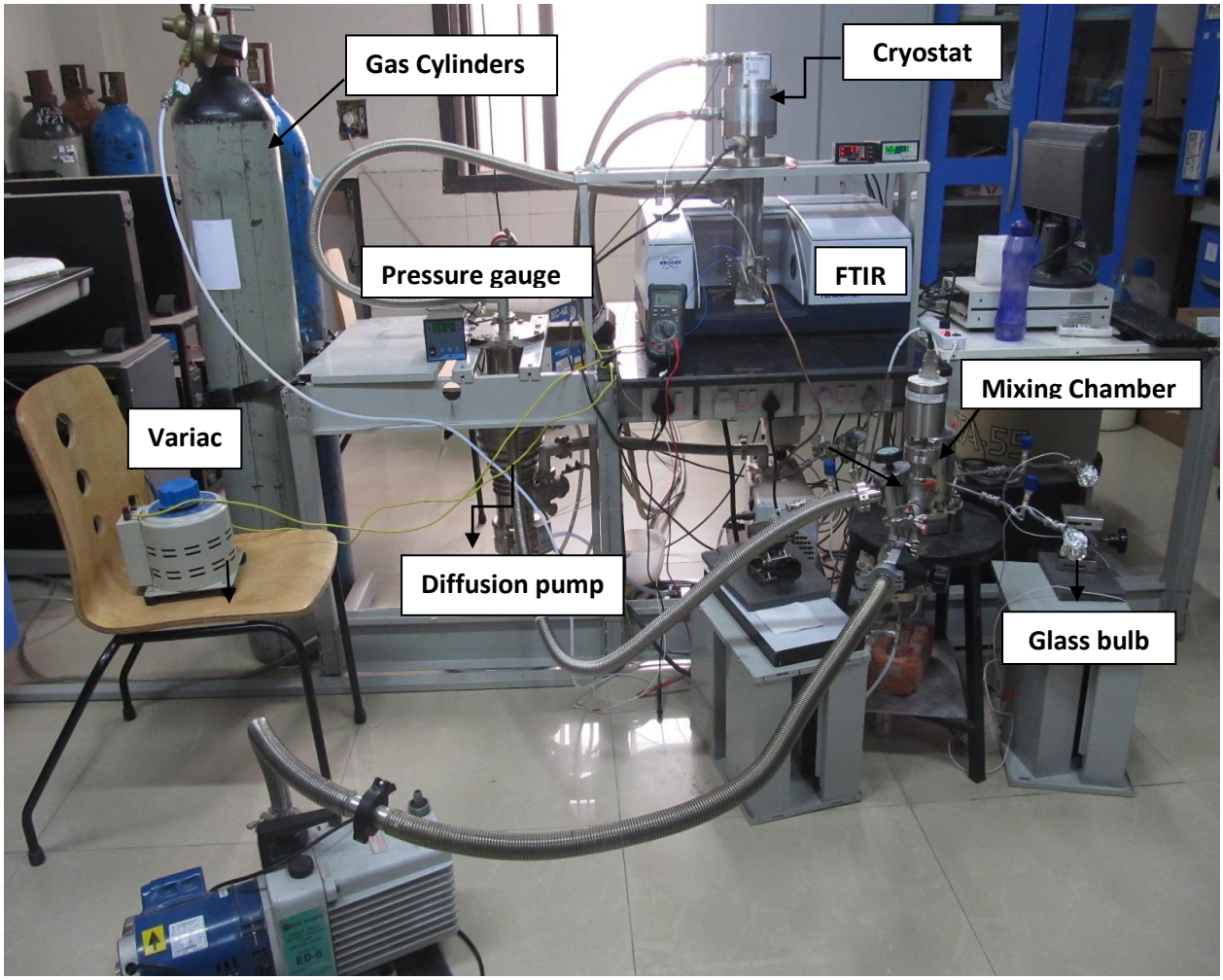

Fig.9: Photograph showing the matrix isolation infrared setup used in this work

2.6.1. Cryostat based on closed cycle Helium Compressor

The four main parts of cryostat are: a) cold head b) Helium compressor c) temperature control unit and d) optical extension set.

Cold head and Helium compressor

The cold head is the basic unit of closed cycle cryostat in Gifford-McMahon (GM) refrigeration cycle. It is connected to compressor by two gas lines and electrical power cable. One of gas lines supplies high pressure helium gas from compressor to cold head, other gas line returns low pressure helium gas from cold head. The compressor provides required helium gas flow rate at high pressure for the cold head to convert into desired refrigeration capacity. The heat generated due to compression of gas of compressor and diffusion pump was removed by chiller. The lowest temperature achieved by helium gas in GM cycle is around 10 K.

Temperature control unit:

A heater coil mounted on cold tip is used to obtain temperature above 12 K. The temperature control unit regulates current through the heater coil. By using temperature control unit, temperature can be varied from 12 K to 300 K. In our cryostat, silicon diode sensor is used to measure the temperature.

Optical extension unit:

The extension unit consist of a substrate holder, radiation shield and vacuum jacket. The substrate holder is attached to cold head of cryostat, which attains a temperature of 12 K. A KBr substrate is mounted on cold substrate holder. Rotation shield is made up of copper and is fixed around the cryotip. The rotatable vacuum jacket has four ports. Another vacuum jacket is attached to this rotatable vacuum jacket through O ring seal. Two of the opposite ports of the rotatable vacuum jacket are fitted with KBr windows. These windows transmit the infrared beam to detector. Third port is fitted with quartz window to transmit UV-Visible light to study photochemistry based on the matrix isolated sample. A sample inlet system is connected to the fourth port, through which deposition is conducted.

2.6.2. Vacuum system:

The cryostat was evacuated by an oil diffusion pump with pumping speed of 280 litres/sec backed by rotary pump. A second rotary pump was used as roughing pump for vacuum system. Both rotary pumps have a pumping speed of 100 litres/min. The base vacuum in system was 10^{-6} mbar and it was measured using cold cathode gauge. The pressure above 10^{-3} mbar was measured using a Pirani gauge.

2.6.3. Vacuum Pyrolysis Setup:

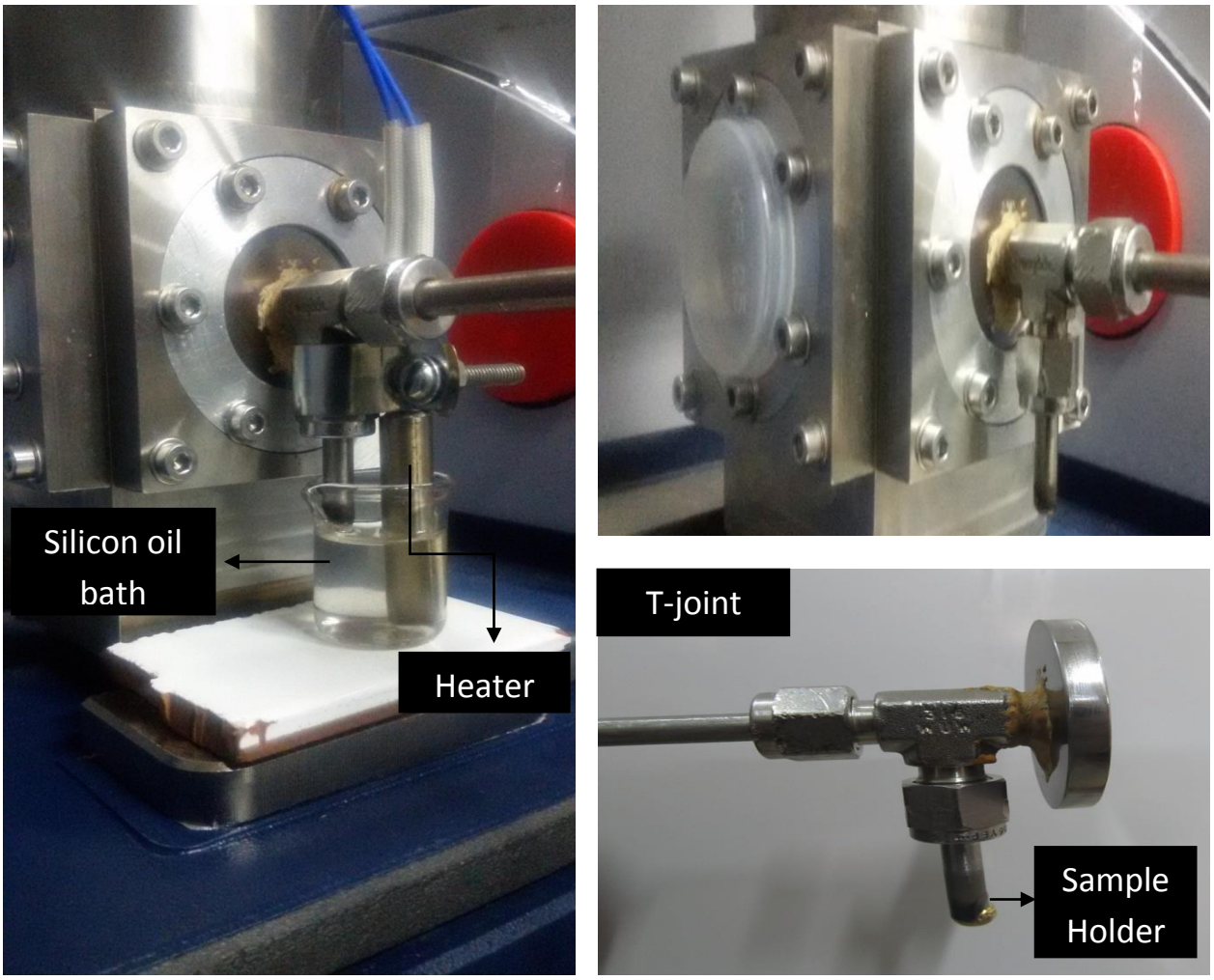

Fig.10. Photograph showing the vacuum pyrolysis setup

In vacuum pyrolysis setup, stainless steel sample holder (3.2 cm in length) was attached to nozzle via T-joint as shown in the **Fig. 10**. Sample holder fitting arrangement was done maintaining a minimum distance from orifice (through which gaseous sample is allowed to effuse into vacuum system) in order to avoid wall collisions and long residence time.

Through this T-joint fitted nozzle, mixing chamber was connected to cryostat. Sample holder was dipped in silicon oil (heating medium) and heated with the help of density small immersion heater. The heater was connected to Variac (Input 240 Volts and Output 0-230 Volts) in order to regulate temperature while heating. The temperature was measured by Platinum Resistance Thermometer (PRT), which was also used as Stirrer in order to ensure uniform heating. With this setup, suitable precursor was pyrolyzed in heated tube held at few milliTorr before deposition.

2.6.4. FTIR spectrometer:

Bruker Tensor 27 FTIR spectrometer was used for our experiments operating at a resolution of 0.50 cm^{-1} for recording the spectrum in the spectral range 4000-400 cm^{-1}.

2.6.5. Sample introduction system:

A mixture of a proton donor solvent (water/methanol) and matrix gas (Ar/N_2) was prepared in a stainless steel mixing chamber of one litre capacity, which was connected to the cryostat through a T-joint fitted nozzle. Sample holder containing 1, 3-dimethylimidazolium-2-carboxylate was heated to decarboxylation temperature. A mixture of water/methanol and matrix gas was effused through the nozzle in order to carry the pyrolyzed 1, 3-dimethylimidazolium-2-carboxylate into vacuum system.

2.7. Experimental procedure:

A carbene precursor i.e., 1, 3-dimethylimidazolium-2-carboxylate was weighed, into the pyrolysis arrangement and pumped down for 5-6 hour to attain pressures of 10^{-6} mbar. In another glass bulb, the coreagent, water or methanol, was taken. The glass bulb was thoroughly degassed prior to solvent (water/methanol) loading. The sample of methanol or water was then subjected to several freeze-pump-thaw cycles before deposition, in order to eliminate any trapped gaseous impurities.

The water/inert gas (or methanol/inert gas) mixture was prepared in a mixing chamber, with various concentrations of the water (or methanol).

Initially, the silicon oil bath was preheated, without dipping the sample holder into the oil, to the desired temperature. Once the desirable temperature was reached, the deposition of the mixture of matrix gas and proton donor solvent (water/methanol) was started. About 3 minutes later, sample holder containing the carbene precursor was inserted into hot oil to initiate the decarboxylation reaction. The products of the decarboxylation were introduced into the vacuum system through a second nozzle. These products and the inert gas/solvent mixture were codeposited onto the cold KBr substrate. The inert gas/solvent mixture was deposited at a rate of ~ 3mmol/hr.

After completion of the deposition, a spectrum was recorded. The KBr substrate was then warmed to 30 K and held at this elevated temperature for 30 minutes and then returned to 12 K. The spectrum of the matrix thus annealed was again recorded. After every experiment, the vacuum system was opened and cleaned before the start of the next experiment.

2.8. Precursor Synthesis and Characterization:

2.8.1. Synthesis of 1, 3-dimethylimidazolium-2-carboxylate:

Overall Reaction:

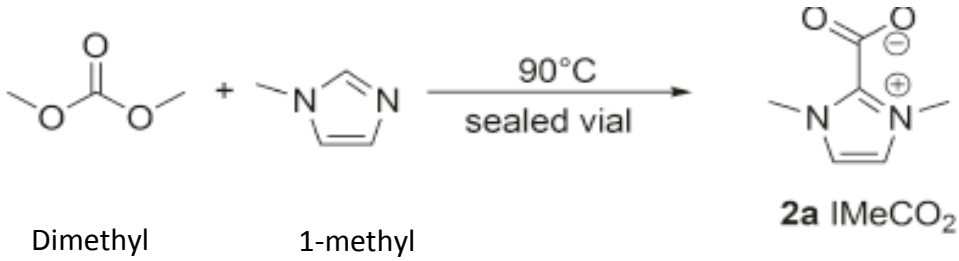

Dimethyl Carbonate

1-methyl imidazole

1, 3-dimethylimidazolium-2-carboxylate

Fig. 11: Scheme of synthesis of 1, 3-dimethylimidazolium-2-carboxylate

The report of Crabtree and co-workers was followed to synthesise 1, 3-dimethylimidazolium-2-carboxylate.[32] A screw-top pressure tube was charged with dimethyl carbonate (3.0 mL), 1-methylimidazole (2 mL) and a stir bar. It was sealed and heated for 30 hours at 90^0C. After approximately 4 hours, the initially clear solution became cloudy with white precipitate, and after 24 hours there was copious amount of white solid in a brown supernatant liquid. The solid was filtered and washed thoroughly with methylene chloride (3x15 mL), acetone (3x15 mL) and ether (2x10 mL). The white solid was isolated with yield of 11 % (377 mg.) The product was characterized by NMR, solid state IR, TGA-MS and Melting point experiments.

^{1}H NMR (400 MHz, D_2O) δ 3.84 (s, 6H, *N*-CH_3), 7.23 (s, 2H, H-4 and H-5).

^{13}C NMR (100 MHz, D_2O) δ 36.69, 123.00, 139.65, 158.25.

2.8.2. TGA-MS characterization of 1, 3-dimethylimidazolium-2-carboxylate:

To determine at what temperature decarboxylation takes place, TGA-MS analysis was carried out. TGA-MS data is also very helpful in exhibiting weight loss corresponding to moisture and other gaseous reaction products as mentioned in **Table 1** below:

Table 1: TGA – MS data of 1, 3-dimethylimidazolium-2-carboxylate

Sr. No	Gaseous species (m/z)	Temp. corresponding to maximum loss ($^{loss}T_{max}$) in ^0C	Change in current value (Room Temp. $\rightarrow$ $^{loss}T_{max}$)
1.	N_2 (14)	267.905823	6.02499e-12 -->9.84754e-11
2.	H_2O (18)	128.951386	3.82548e-9 -->5.87638e-9
3.	CO (28)	265.907471	2.14947e-10 -->7.403864e-10
4.	CH_4 (32)	268.631226	6.90104e-11 --> 4.90186e-10
5.	**CO_2 (44)**	**264.345581**	**5.50746e-11-->2.424456e-9**

From TGA-MS data, it was very clear that increase in factor of 10^2 for current value corresponding to CO_2 confirms the decarboxylation. The MS fragment ion curve for CO_2 (m/z =44) displays peak as result of decarboxylation as shown in **Fig. 12**.

From this analysis, it was determined that the decarboxylation is maximum at 264 ^0C. However, from our experiments it was evident that perceptible decomposition occurred even at 60 ^0C.

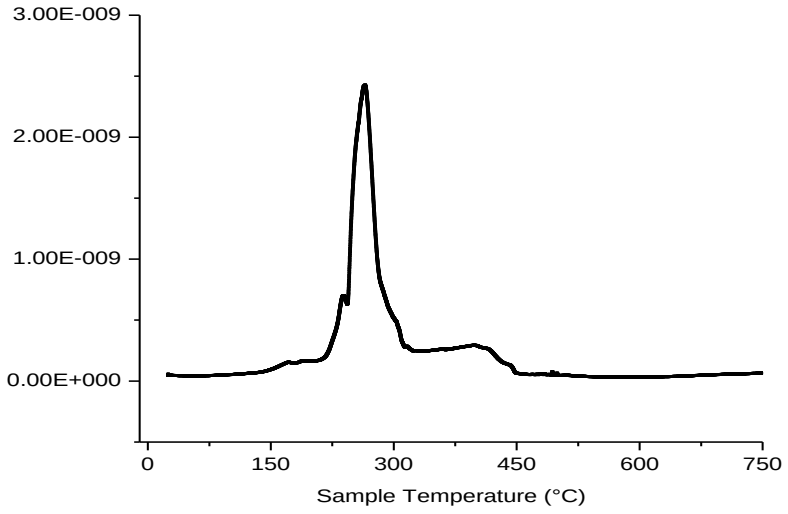

Fig. 12: TGA-MS spectrum of 1, 3-dimethylimidazolium-2-carboxylate

2.9. Computational Procedure:

The computational study was carried out using Gaussian 09 package[33] in Linux operating system. Molecular properties such as structures, energies and frequencies were calculated to verify our experimental results. To examine the nature of interactions between the monomers of complexes, AIM (Atoms-In-Molecule)[34] package was also used.

Hartree-Fock methods (HF), Density Functional Theorem (DFT), Møller-Plesset perturbation theory(MP_n) (where n denotes the order of perturbation), Configuration interaction (CI), Coupled cluster (CC), Multi-configurational self-consistent field (MCSCF), etc. are some of the popular electron structure methods used for *ab-initio* calculations.

Electron density, which is a function of just three variables (x, y, z), is used to determine all electronic properties of system in DFT. The BLYP (Becke-Lee-Yang-Parr) is one of such functional which includes some HF exchange. It involves both electron spin densities and their gradients. Hybrid functionals define the exchange functional as a linear combination of HF, local and gradient corrected exchange terms. The most used such functional is B3LYP. The B3LYP method uses the Becke-three parameter non-local exchange functionals[35, 36] with non-local correlation of Lee at al. DFT is more accurate than HF, since it includes electron correlation. An iterative self-consistent field method is used to calculate energy and orbital coefficients. It is an appropriate method for systems having up to 100 atoms. But recently, advance modifications in DFT functionals have been introduced, named as Minnesota functional (M06). Some strategies are used in designing M06 and these are constraint satisfaction, modelling the exchange correlation hole, empirical fits and mixing HF and approximate DFT exchanges[37]. Møller-Plesset perturbation theory (MP) is a post HF *ab-initio* method. It improves on the HF method by adding electron correlation effects by means of Rayleigh-Schrodinger perturbation theory to second (MP2), third (MP3) and fourth order (MP4).

2.9.1. Geometry optimization and frequency calculation:

A geometry optimization is done to obtain molecular structure corresponding to a minimum on the potential surface. A geometry optimization starts with the guess molecular

structure specified as inputs, and the steps along the potential energy surface. The energy and gradient are first computed at the point on the potential surface corresponding to initial geometry. This information is used to determine how far and in which direction the next step is taken to improve the geometry. The forces will be zero at the minimum or at the stationary point. The optimization was achieved when the forces, the root mean square forces, the calculated displacement and the root mean square of the displacement for the subsequent step are below the present threshold values.

Frequency calculations were performed at the same level of theory used for geometry optimization. Vibrational frequency computations were done to ensure that the computed structures did correspond to minima on the potential surface and also to assign the vibrational features observed in the experiments. For the purpose of comparison with experimental results, the computed vibrational frequencies were scaled. The scaling factor was calculated by correlating the experimentally observed strongest feature with the strongest feature indicated by the computations in the spectral region of interest. The scaling factor that will bring the computed frequency in good agreement with that of experiment will then be used to scale all other vibrational frequencies. The computed scaled frequencies will be used to simulate the vibrational spectra. The synthetic spectra were generated assuming a full width at half maximum of 1 cm^{-1}. Zero point vibrational energies (ZPE) obtained from frequency calculations were used to calculate ZPE corrected energies.

2.9.2. Stabilization energy calculation of complexes:

The stabilization energy (ΔE) of the complex is given by $\Delta E = E_{AB} - (E_A+E_B)$. Where, E_A, E_B and E_{AB} represent the energies for monomers A, B and the complex AB respectively. If the value of ΔE is negative, the complex is more stable relative to precursors. The stabilization energy of the complex for the zero point energy (ZPE) was also calculated.

It has been observed that the stabilization energy becomes less negative after the zero point correction. The zero point vibrational energy (ZPE) is equal to one half the sum of the vibrational fundamental frequencies. It can be easily seen that in the complex there are six normal modes more than the sum of the normal modes of the two monomers. Consider that the two monomers of the complex have N_1 and N_2 of atoms respectively, in which case

the complex will have (N_1 + N_2) atoms. Assuming that both the monomers and the complex are non-linear molecules, the number of extra normal modes can be calculated as follows:

Extra normal modes = $[3(N_1+N_2)-6] – [(3N_1-6) + (3N_2-6)]$
Therefore, one half of the sum of vibrational frequencies of six extra normal modes is responsible to make stabilization energy less negative.

When the energy of complex (E_{AB}) is computed, the basis functions used are those of both the monomer subunits. Whereas, for computing the energy of individual monomers (E_A and E_B), the basis functions pertaining to only the corresponding monomers are used. As the number of basis function used is larger in the computation of complex, the energy obtained will be lower. In complex, basically each monomer can use the basis functions of other. Stabilization energies thus derived from the calculated energies E_A, E_B and E_{AB} will be overestimated and the error is referred to as the basis set superposition error (BSSE). The best way to eliminate BSSE is to increase the basis set until the stabilization energy is stable to desired accuracy. The commonly used method to correct for BSSE is by counterpoise correction proposed by Boys and Bernadi.[38] In this scheme, the energies of monomer E_A and E_B and the complex E_{AB} are calculated in the same basis set spanned by the functions of the complex AB and the difference is obtained as follows:

$\Delta E = E_{AB}(AB) – [E_A(AB) + E_B(AB)]$
where, E_A = Energy of the monomer A using the basis set AB
E_B = Energy of the monomer B using the basis set AB
E_{AB} = Energy of the complex AB using the basis set AB.

BSSE corrected term is evaluated as follows:
BSSE correction = $\{[E_A(A) – E_A(AB)] + [E_B(B) – E_B(AB)]\}$
The BSSE correction term turns out to be positive. When this term is added to the raw stabilization energy, a negative quantity, overall BSSE corrected BSSE energy becomes less negative.

2.9.3. Atoms-in-Molecule methodology:

Atoms in molecules theory was first proposed by Bader, which uses an analysis of the electron density topology[39]. The Gaussian 09 package generates the wave function corresponding to the optimized geometry of a molecule or complex. Bond critical points, charge density (ρ) and Laplacian of charge density are obtained from the electron density plots. The charge density, ρ(r), is a physical quantity which has a definite value at each point in space. It is a scalar field defined over three dimensional space. Each topological feature of ρ(r), whether it is a maximum, a minimum, or a saddle point, has associated with it in a space called a critical point. At critical point, the first derivative of ρ(r) vanishes. The sign of its second derivative or curvature at this point determines whether a function is maximum or minimum. The topological properties of such a scalar field are summarized in terms of the number and nature of its critical points. The number of non-zero eigenvalues at the critical point is termed as a rank of critical point and is denoted of ω. The signature is the algebraic sum of signs of eigenvalues and is denoted by σ. The critical point is labelled by giving the values (ω, σ). For example, (3,-1) critical point means, three non-zero curvatures and one positive and two negative eigenvalues. A (3, -1) critical point correspond to a bond between two atoms, a (3, +1) critical point to a ring, a (3, +3) critical point to a cage and a (3, -3) critical point corresponds to a maximum.

The sum of three Hessians (λ_1, λ_2, λ_3) at a bond critical point, the Laplacian quantity, provides a useful characterization of the manner in which the electronic charge density is distributed in the internuclear region. If the value of charge density ρ ($<10^{-1}$a.u.) and the curvature of charge density are large, Laplacian of charge density may be positive or negative usually in the same order of magnitude as ρ then the interaction is of shared type, typical of covalent interaction. For the closed shell interactions, such as hydrogen bond complexes, van der Waals complexes and ionic systems, the charge density ($\sim10^{-2}$ to 10^{-3}a.u.) at the bond critical point is quite small and the Laplacian of the charge density is positive.

Chapter 3

Result and Discussion

The hydrogen bonded complexes between 1, 3-dimethylimidazol-2-ylidene i.e., N-Heterocyclic carbene (NHC) and proton donor solvents like water and methanol were studied using both computation and experimental techniques. These hydrogen bonded complexes are proposed to be studied experimentally using matrix isolation infrared spectroscopy. The nucleophilic nature of 1, 3-dimethylimidazol-2-ylidene carbene carbon provides opportunity to investigate hydrogen bonding interactions. It has one hydrogen acceptor and one hydrogen donor site. On the other hand, each of the proton donor solvents like water and methanol has one hydrogen donor and one acceptor site. Hence, these systems were expected to show interesting hydrogen bonding scenario.

From the comparison of 1, 3-dimethylimidazol-2-ylidene monomer experimental spectrum with the spectrum obtained from scaled frequencies of 1, 3-dimethylimidazol-2-ylidene, it was concluded that 1, 3-dimethylimidazol-2-ylidene i.e., N-heterocyclic carbene, was deposited into the matrix, without any rearrangement. The spectra of scaled frequencies were plotted using a general spectrum synthesis program, Synspec. Since, the 1, 3-dimethylimidazol-2-ylidene was obtained by the vacuum pyrolysis of its precursor 1, 3-dimethylimidazolium-2-carboxylate. Hence, experimental spectrum of the monomer was also compared with the spectrum obtained from the scaled frequencies of its precursor. The experimental spectrum of the N-heterocyclic carbene matches with that of computed spectra but does not matches with the carboxylate precursor **Fig. 13**. An intense peak corresponding to asymmetric stretching vibration of free CO_2 at 2349.0 cm^{-1} in the spectrum clearly indicates the decarboxylation of 1, 3-dimethylimidazolium-2carboxylate.The frequency comparison of computed and experimental data for 1, 3-dimethylimidazol-2-ylidene is given in **Table 2**.

As mentioned earlier, the mixture of vacuum pyrolyzed 1, 3-dimethylimidazolium-2-carboxylate and a proton donor solvent (water or methanol) was co-

deposited in both $N_2$and Ar matrices. A deposition was usually conducted for about 3 hours, during which time about 150 Torr of inert gas (N_2/Ar) was deposited into the matrix. The ratio of sample deposited into the matrix to inert gas is approximately 1:1000. The frequency calculations were performed using the R-B3LYP/6-311++G (d, p) level of theory. All frequencies were found to be real, which confirms that structures obtained were minima on the potential energy surface.

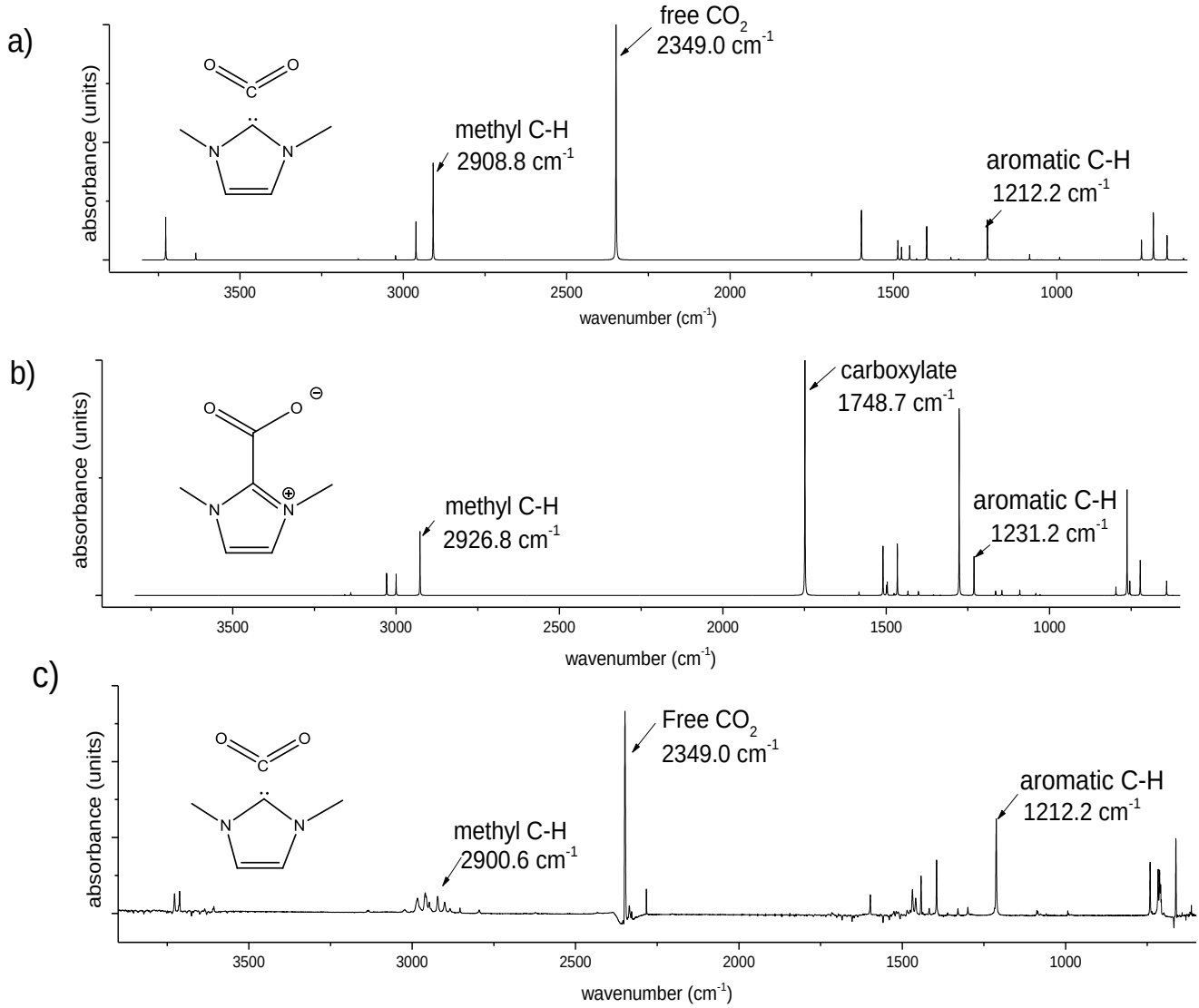

Fig. 13: (a) Computed IR spectrum of 1, 3-dimethylimidazol-2-ylidene and free CO_2 (b) Computed IR spectrum of 1, 3-dimethylimidazolium-2-carboxylate (c) Experimental IR spectrum of vacuum pyrolyzed 1, 3-dimethylimidazolium-2-carboxylate trapped in a solid nitrogen matrix at 12 K

Table 2: Calculated IR vibrational wavenumbers (cm^{-1}) of (1) 1, 3-dimethylimidazol-2-ylidene and (2) 1, 3-dimethylimidazolium-2-carboxylate, and (3) experimental (N_2, 12 K) IR spectrum of vacuum pyrolyzed 1, 3-dimethylimidazolium-2-carboxylate trapped in solid N_2 matrix at 12 K. Computed intensities are given in parenthesis in Km/mol.

Sr. No	$\bar{\upsilon}_{calcd}$ **(1)**	$\bar{\upsilon}_{scaled}$	$\bar{\upsilon}_{calcd}$ **(2)**	$\bar{\upsilon}_{scaled}$	$\bar{\upsilon}_{exp}$ **(3)**	Mode of assignment
1	617.5 (2.38)	612.0			615.1 (0.07)	
2			647.5 (19.04)	641.8	-----	
3					662.4 (0.51)	bend.str.CO_2
4	710.6 (63.06)	704.3			707.3 (0.30)	
5			729.0 (47.18)	722.5	-----	
6	747.3 (26.93)	740.7			741.5 (0.35)	
7			769.6 (142.23)	762.8	-----	
8			803.9 (11.68)	796.8	-----	
9	1097.6 (7.28)	1083.2	1105.5 (7.45)	1091.0	1085.1,1088.1(0.04)	
10	1228.2 (54.00)	1212.2			1212.2 (0.64)	
11			1247.6 (52.57)	1231.2	-----	
12			1293.6 (250.53)	1276.6	-----	
13	1317.7(1.46)	1300.4			1299.4 (0.05)	
14	1341.7 (3.67)	1324.1			1329.9 (0.05)	
15	1416.7 (44.88)	1398.1	1420.1 (5.25)	1401.4	1395.0 (0.37)	
16	1469.6 (19.43)	1450.3	1452.6 (5.75)	1433.5	1442.6 (0.26)	
17	1494.9 (16.81)	1475.3	1485.3 (68.97)	1465.8	1459.0 (0.12)	
18	1506.3 (25.92)	1486.5	1495.7 (2.76)	1476.1	1469.1 (0.17)	
19			1529.8 (65.90)	1509.7	-----	
20					1597.9 (0.13)	bend. str.H_2O
21			1772.0 (524.42)	1748.7	-----	
22					2283.3 (0.17)	$^{13}CO_2$ dimer
23					2349.0 (1.41)	Asym. str.CO_2
24	3030.1 (129.59)	2908.8			2900.6 (0.07)	
25			3048.8 (74.39)	2926.8	-----	
26	3084.9 (51.32)	2961.5			2960.5 (0.13)	
27			3125.0 (15.15)	3000.0	-----	
28			3125.2 (13.66)	3000.1	-----	
29	3149.8 (5.77)	3023.8	3154.4 (6.08)	3028.2	3024.3 (0.02)	
30	3268.9 (2.09)	3138.2	3269.6 (4.15)	3138.8	3133.9,3138.2(0.01)	
31					3607.6(0.04),3609.6 (0.02), 3711.9 (0.13)	CO_2 combinations
32					3727.3 (0.11)	Asym.str.H_2O

3.1. NHC – Water complexes:

3.1.1. Computation

The possible complexes which can be formed from 1, 3-dimethylimidazol-2-ylidene and water (as shown in **Fig. 14**) are listed below:

1) Complex 1 (NHC-W1) – Hydrogen of water acts as proton donor to the carbene carbon in 1, 3-dimethylimidaol-2-ylidene.
2) Complex 2 (NHC-W2) – Oxygen of water acts as proton acceptor to the hydrogen attached to doubly bonded carbon in 1, 3-dimethylimidaol-2-ylidene.

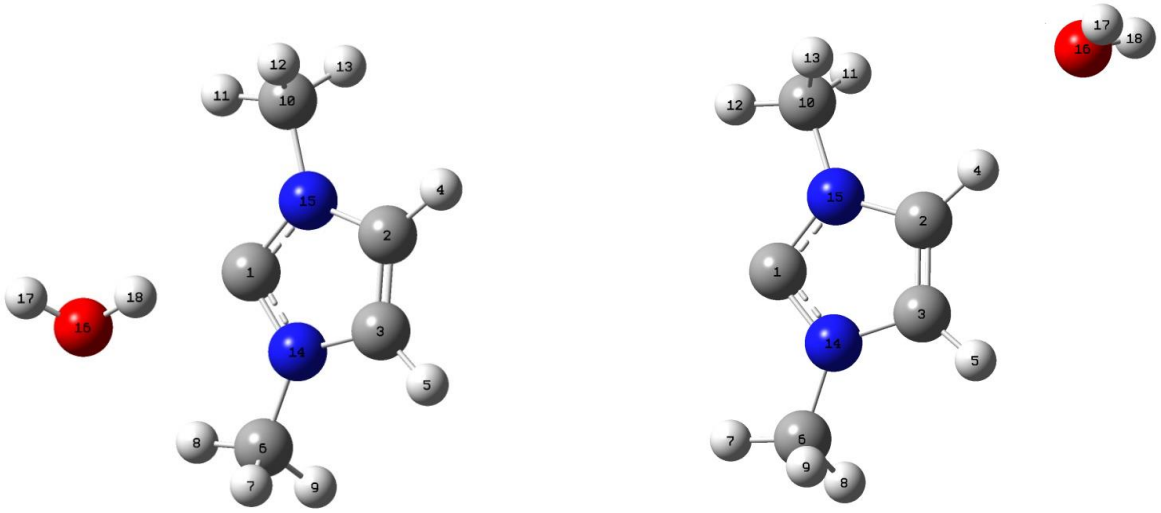

Complex 1 Complex 2

Figure 14: Structures of optimized geometries obtained for the two different complexes of 1, 3-dimethylimidazol-2-ylidene and water, computed at R-B3LYP/6-311++G (d, p) level of theory.

At the R-B3LYP/6-311++G (d, p) level of theory, both possible complexes were obtained between 1, 3-dimethylimidazol-2-ylidene and water which are shown in the **Fig. 14**; namely complex 1 and complex 2. The stabilization energy of these two complexes was

computed after individually correcting for ZPE and BSSE as shown in **Table 3**. At this level of theory, it is clear that complex 1 is significantly more stable compared with complex 2. The important structural parameters for these two complexes are indicated in **Table 4**.

Table 3: Computed stabilization energies (in kcal mol^{-1}) of 1, 3-dimethylimidazol-2-ylidene and water complexes at R-B3LYP/6-311++G (d, p) level of theory

Complex	ΔE_{RAW}	ΔE_{ZPE}	ΔE_{BSSE}
Complex 1 (NHC-W1)	-9.6	-7.6	-9.1
Complex 2 (NHC-W2)	-2.4	-1.4	-1.7

Table 4: Important structural complex parameters, bond lengths (Å), bond angles (°) and dihedral angles (°), of 1, 3-dimethylimidazol-2-ylidene and water complexes (as shown in Fig. 14), computed at the R-B3LYP/6-311++G (d,p) level of theory

Complex Parameters	**Complex 1**	**Complex 2**
r(C1-H18)	1.97	---
r(H4-O16)	---	2.33
r(O16-H18)	0.98	0.96
r(O16-H17)	0.96	0.96
r(C1-N15)	1.36	1.37
r(C2-C3)	1.35	1.35
N14-C1-H18	114.25	---
N15-C1-H18	142.62	---
C1-H18-O16	164.35	---
H4-O16-H18	---	123.80
H4-O16-H17	---	123.79
C2-H4-O16	---	173.32
N14-C1-N15	103.00	102.15
H17-O16-H18-C1	133.57	---
N15-C1-H18-O16	171.64	---
H18-C1-N15-C10	4.39	---
C2-H4-O16-H17	---	107.03
C3-C2-H4-O16	---	179.92
N15-C2-H4-O16	---	-0.07

AIM analysis

An examination of charge density topology was performed using the atoms-in-molecules (AIM) theory of Bader. (3,-1) bond critical points and (3, +1) ring critical points that could be associated with the complexes were located. The electron density ρ (r_c) and Laplacian (L) of electron density $-\hbar^2\nabla^2/4$ (r_c) for complex 1 and complex 2 were computed for the critical points and the values are shown in **Table 5**. The large value of electron density for a critical point indicated the strength of non-covalent interaction present at the corresponding sites in the complexes **Fig.15**.

Table 5: AIM calculations for 1, 3-dimethylimidazol-2-ylidene and water complexes at R-B3LYP/ 6-311++G (d, p) level of theory

Complex	ρ (r_c) in a.u.	L (r_c) in a.u.
Complex 1 (NHC-W1) **(1)**	0.03370	-0.01639
(2)	0.00794	-0.00666
Complex 2 (NHC-W2)	0.01123	-0.00969

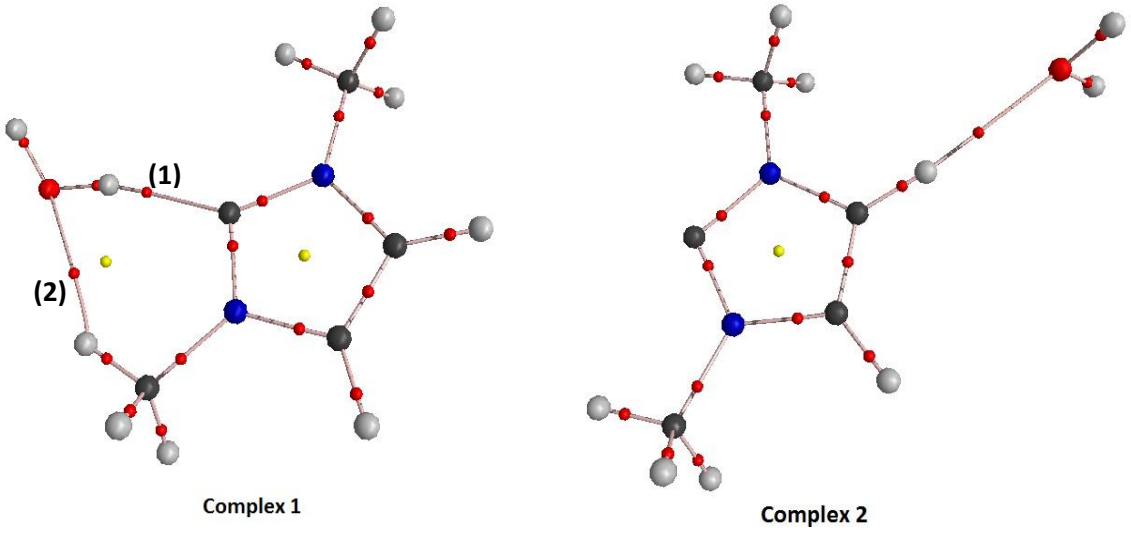

Figure 15: Structures of 1, 3-dimethylimidazol-2-ylidene and water complexes showing the bond critical points, computed at R-B3LYP/6-311++G (d, p) level of theory

3.1.2. Experimental and Vibrational analysis:

The spectra obtained for 1, 3-dimethylimidazol-2-ylidene (NHC) in both N_2 and Ar matrices are as shown in **Fig. 16**. The spectral region depicted in this figure is between 2750 and 3850 cm^{-1}. In this spectral region, features corresponding to the complexes of NHC with water or methanol were observed. Since traces of moisture was always present in the carbene precursor, 1, 3-dimethylimidazolium-2-carboxylate, peaks at 3727.3 cm^{-1} and 3731.6 cm^{-1} corresponding to asymmetric stretch of O-H of water were observed in both N_2 and Ar matrices respectively. In case of N_2 matrix, annealing was done at 30 K, whereas 35 K was annealing temperature for Ar matrix. Spectral subtraction (SS) was done in which spectrum at 12 K was subtracted from annealed spectrum in order to locate any new feature. Bands pointing upwards are assigned to complex features.

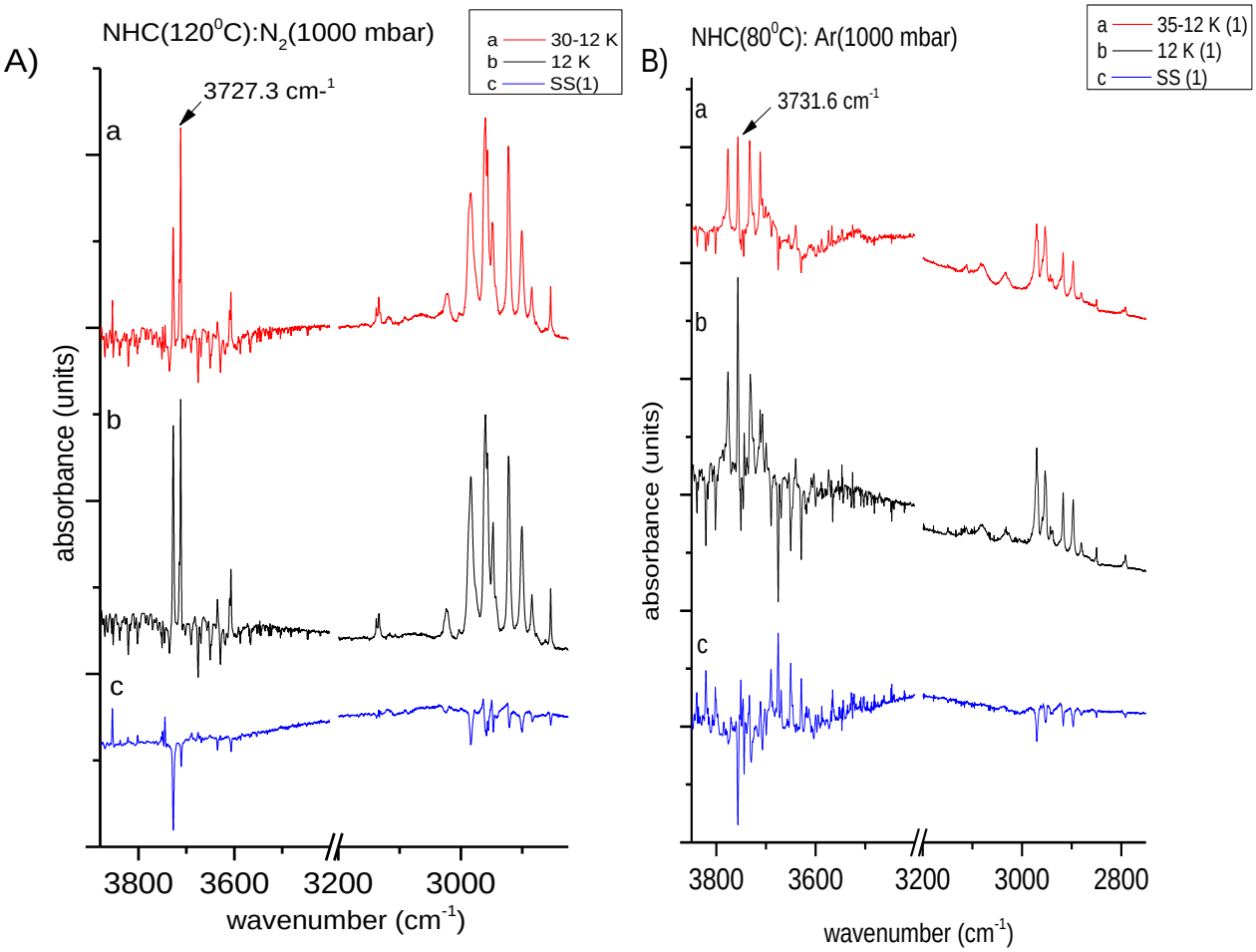

Fig. 16: IR Spectra of NHC in (A) Nitrogen and (B) Argon matrix: (a) after annealing at 30 K in Nitrogen and 35 K in Argon matrix (b) at 12 K (c) spectral subtraction (SS)

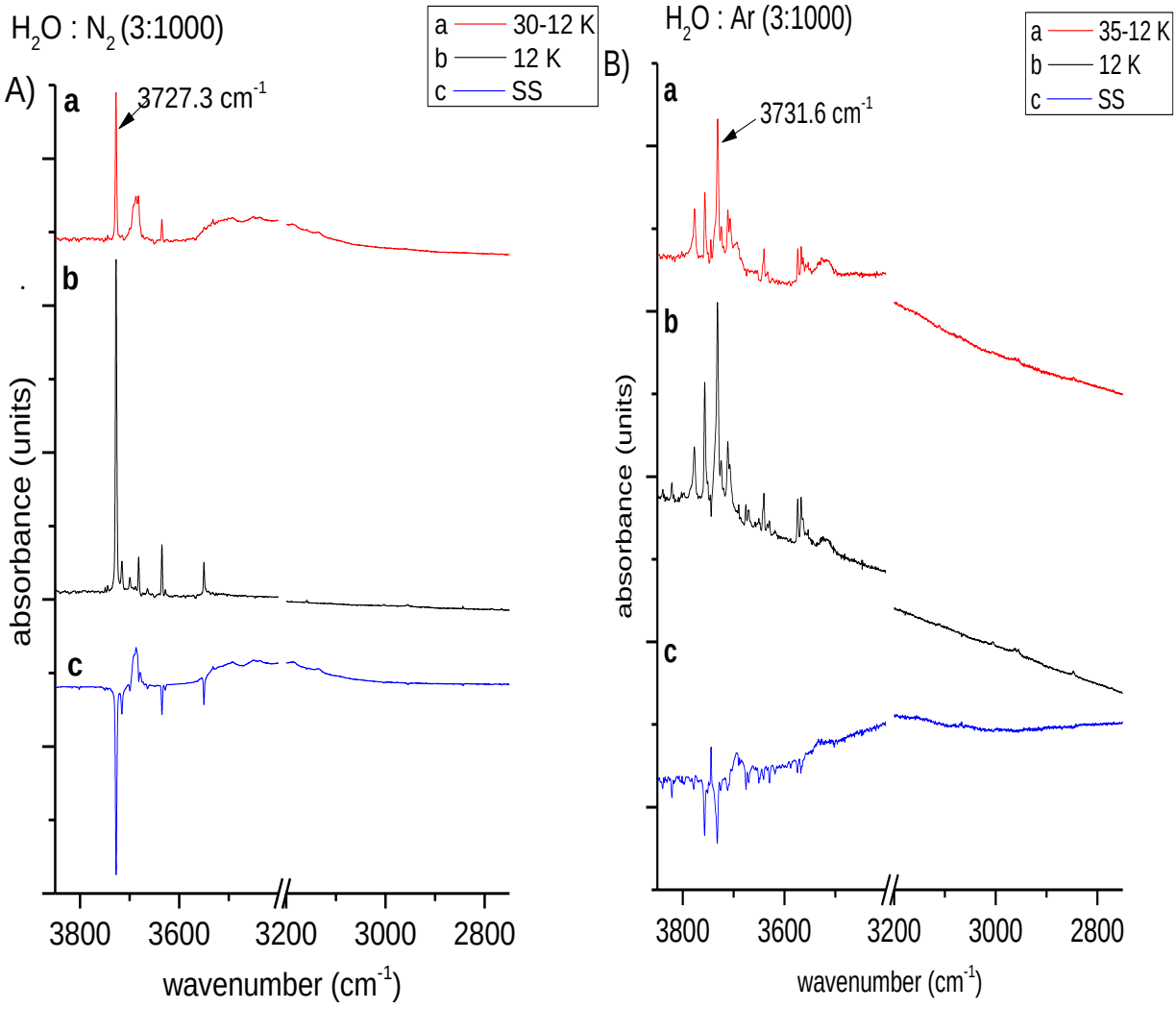

Fig. 17: IR Spectra of Water in (A) Nitrogen and (B) Argon matrix: (a) after annealing at 30 K in Nitrogen and at 35 K in Argon matrix (b) at 12 K (c) spectral subtraction (SS)

Fig.17 shows the spectra obtained for 3:1000 concentration of water, where peaks at 3727.3 cm^{-1} and 3731.6 cm^{-1} corresponds to asymmetric stretch of O-H of water in N_2 and Ar matrices respectively.

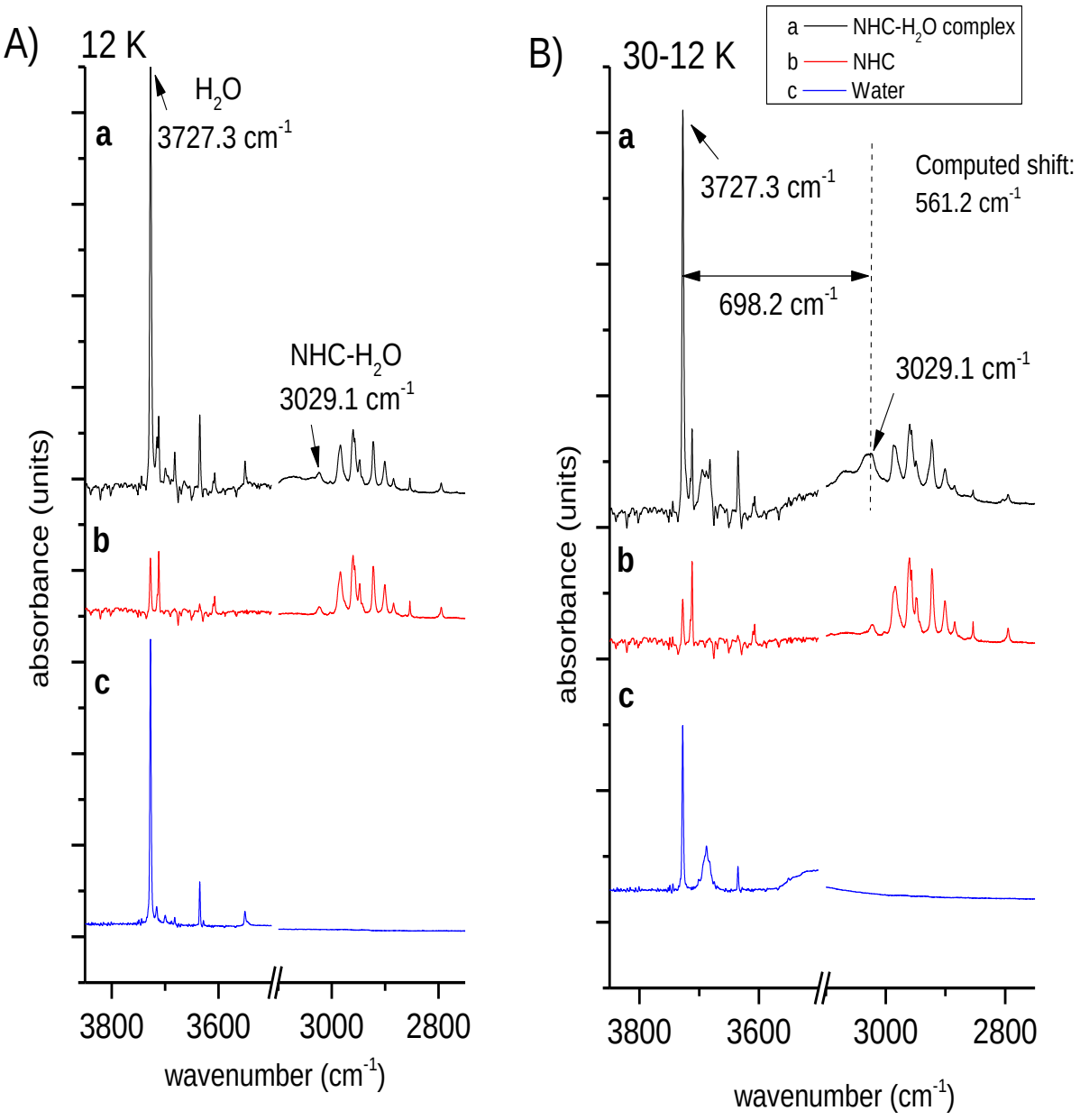

Fig. 18: Comparison of Complex, NHC and H_2O spectra (A) before annealing and (B) after annealing: (a) NHC (120^0C): H_2O: N_2 (3:1000) (b) NHC precursor pyrolyzed at 120^0C (c) H_2O:N_2 (3:1000)

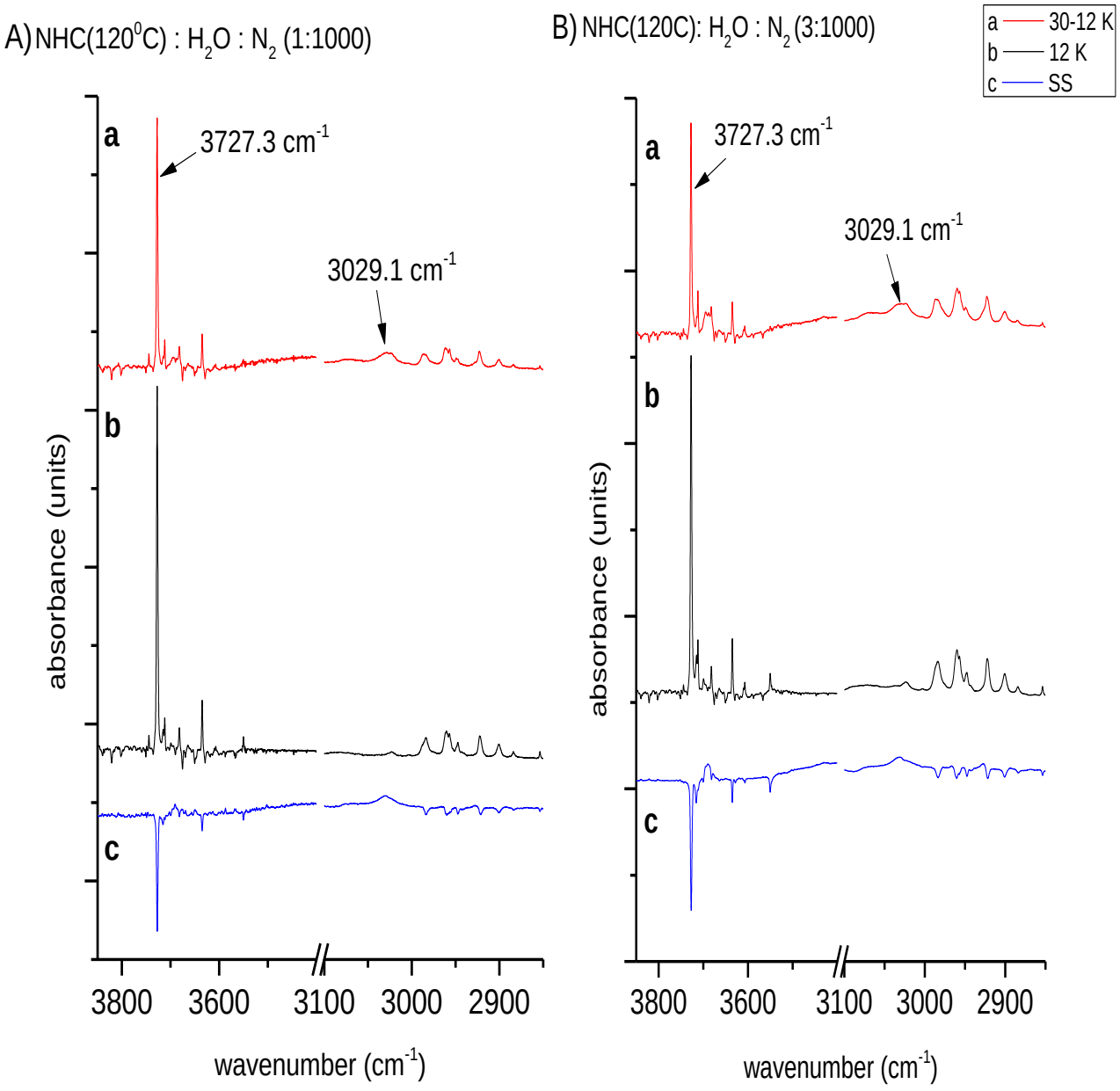

Fig. 19: IR Spectra of NHC- H_2O complex showing concentration dependence of H_2O: N_2 {(A) 1:1000 and (B) 3:1000} (a) after annealing at 30 K (b) at 12 K (c) spectral subtraction (SS)

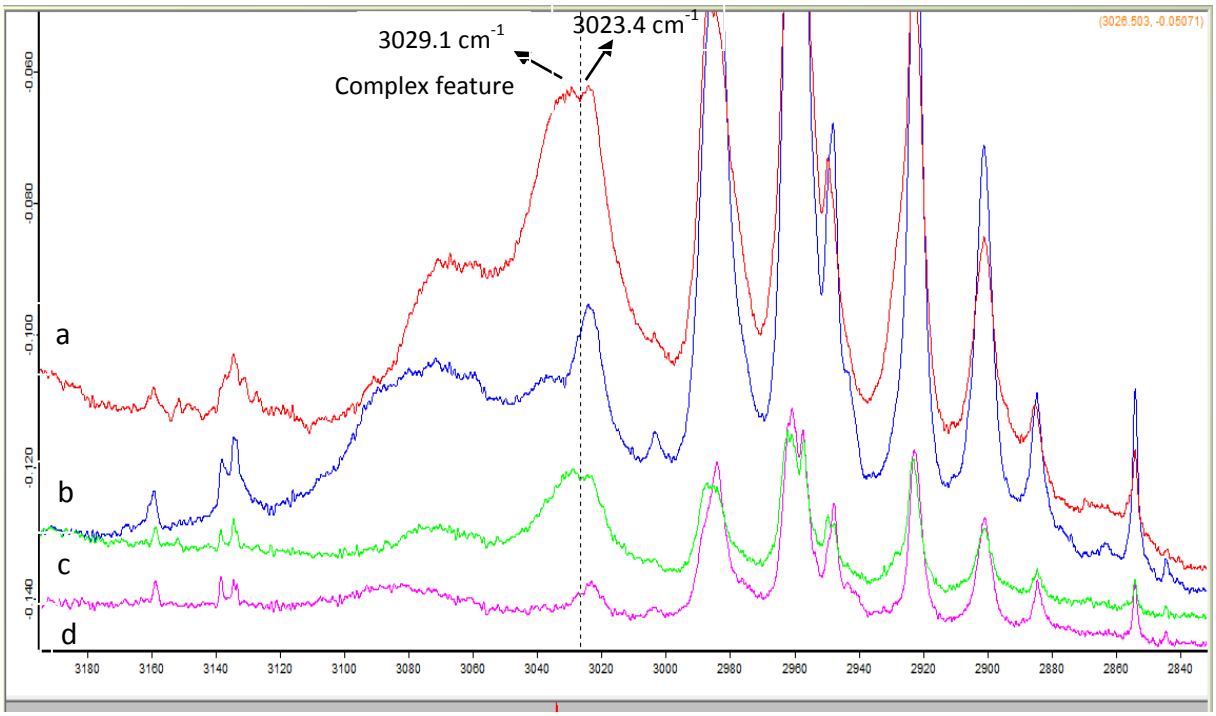

Fig. 20: Resolving the complex feature from monomer (NHC) feature in N_2 matrix: For 3:1000 (H_2O:N_2) concentration (a) after annealing at 30 K (b) at 12 K. For 1:1000 (H_2O:N_2) concentration (c) after annealing at 30 K (d) at 12 K

In Nitrogen matrix, the NHC – H_2O complex feature appeared at 3029.1 cm^{-1} which is not observed in the monomer spectra i.e., NHC and water (**Fig. 18**). This peak also increases in intensity after annealing and as the water concentration is increased three times as shown in the **Fig. 19**. It is clear from the spectral subtraction that complex feature increases in intensity after annealing. Another peak at 3023.4 cm^{-1} also increases after annealing as shown in the **Fig. 20**, but this peak was already there in 12 K complex spectrum as well as NHC spectrum. Hence, it cannot be assigned to complex feature.

Two possible complexes were computed between NHC and water as shown in the **Fig. 14**, namely complex 1 and complex 2. Out of these two complexes, complex 1 is more stable than complex 2 **Table 3**. Therefore, it is likely that complex 1 is observed experimentally. A large red shift of 698.2 cm^{-1} was observed experimentally for the complex in N_2 matrix. It is clear from **Fig. 21** that this experimentally observed red shift (698.2 cm^{-1}) is reasonably good agreement with the computed red shift of complex 1 (561.2 cm^{-1}) than

that of complex 2 (4.9 cm^{-1}). Hence, experimentally observed complex feature is assigned as hydrogen bonded feature due to complex 1.

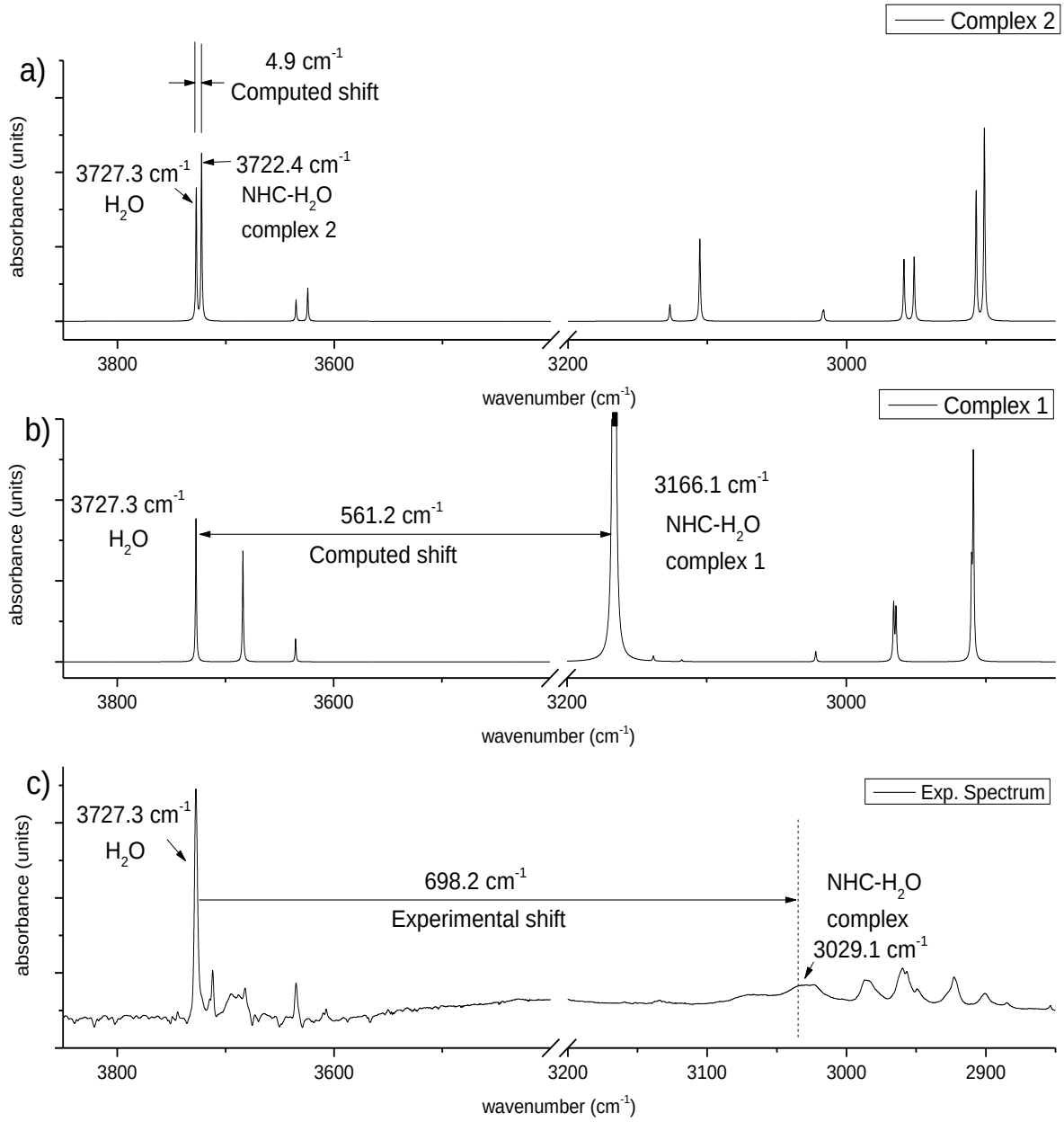

Fig. 21: (a) Computed IR spectrum of NHC-H_2O complex 2 (b) Computed IR spectrum of NHC-H_2O complex 1 (c) Experimental IR spectrum of NHC-H_2O complex trapped in a solid nitrogen matrix at 12 K

Similar experiments were performed in Ar matrix to ensure that complex feature observed in N_2 matrix is not due to site effect. In Argon matrix, peak at 3019.4 cm^{-1} can be assigned as complex 1 feature which is not observed in either of NHC and water spectra **Fig. 22** and **Fig. 23**. But, this peak does not increase in intensity after annealing. There is a possibility that complex has already formed before deposition of reagents.

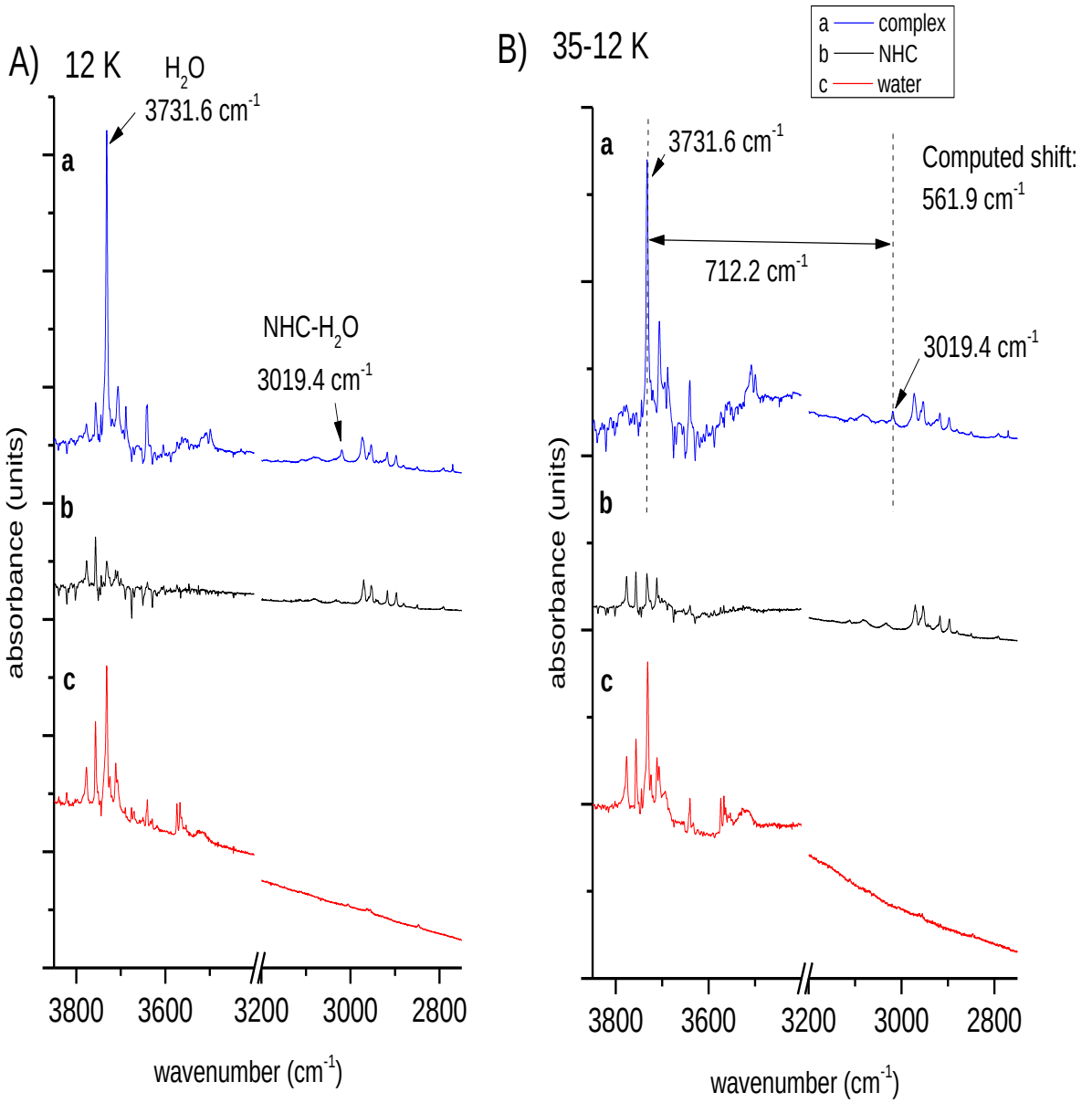

Fig. 22: Comparison of Complex, NHC and H_2O spectra (A) before annealing and (B) after annealing: (a) NHC (80^0C): H_2O: Ar (3:1000) (b) NHC precursor pyrolyzed at 80^0C (c) H_2O: Ar (3:1000)

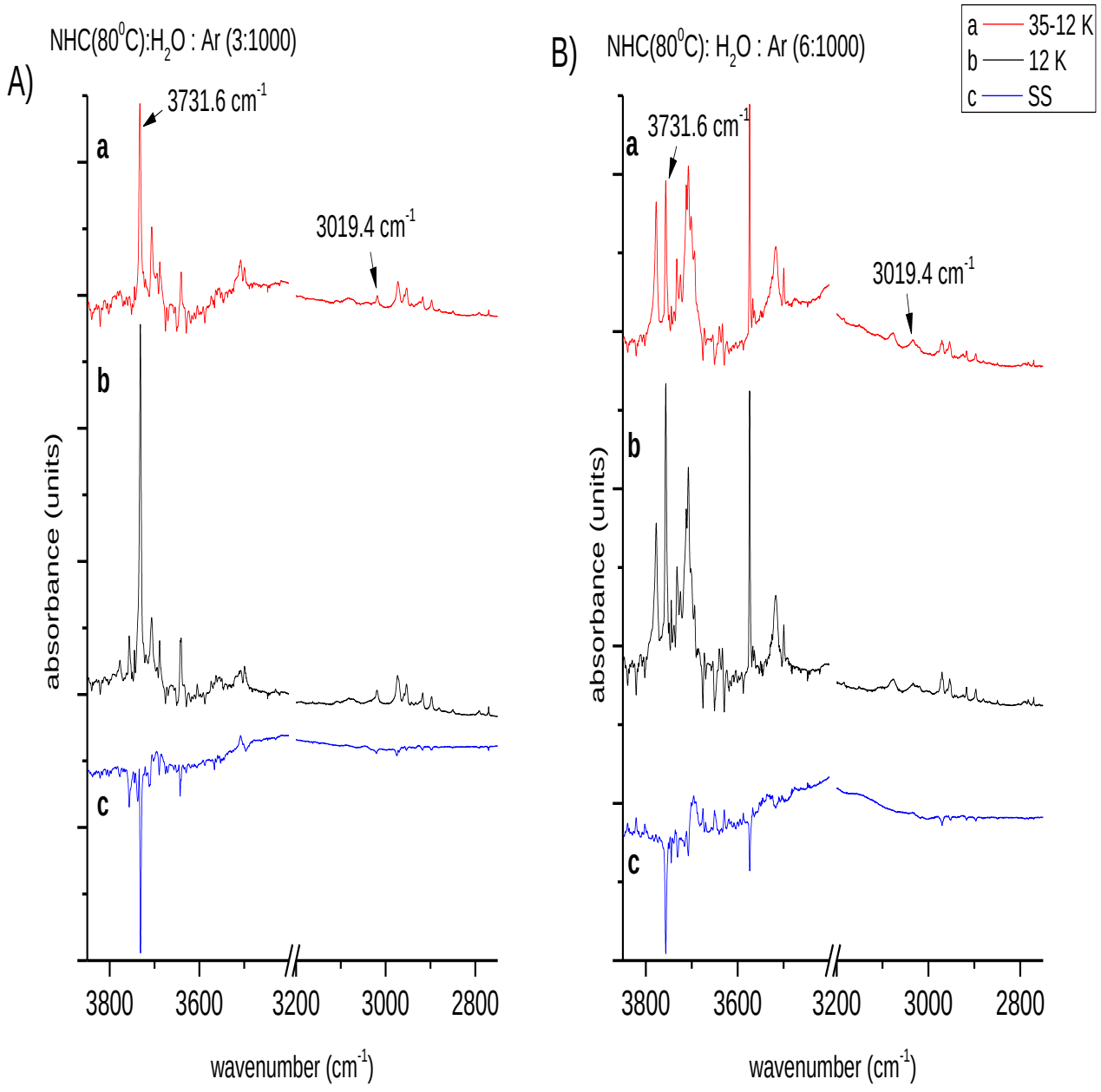

Fig. 23: IR Spectra of NHC- H_2O complex showing concentration dependence of H_2O: Ar {(A) 3:1000 and (B) 6:1000} (a) after annealing at 35 K (b) at 12 K (c) spectral subtraction (SS)

In complex 1, as soon as hydrogen of water forms a hydrogen bond with carbene carbon, water molecule loses its symmetry. There are no more symmetric and asymmetric stretching vibrations in the complex. Instead, we have bound and unbound O-H stretches. As per the computational calculations at R-B3LYP/ 6-311++G (d, p), the intensity of unbound O-H stretch in complex 1 was found to be pretty less compared to the bound O-H stretch. A feature corresponding to this unbound stretch was not observed experimentally. The experimental and computed frequencies for NHC – Water complexes are as indicated in **Table 6**. A large red shift of 698.2 cm^{-1} was observed experimentally in case of complex 1 in N_2 matrix, whereas a red shift of 712.2 cm^{-1} was observed for the same in Ar matrix.

Table 6: Experimental and computed frequencies for NHC-H_2O complexes at R-B3LYP/ 6-311++G (d, p) level of theory in both N_2 and Ar matrices

Nitrogen matrix	Calculated frequencies (cm^{-1})	Scaled frequencies (cm^{-1})	Scaling factor	Experimental frequencies (cm^{-1})	Computed shift (cm^{-1})	Experimental shift (cm^{-1})	Mode of assignment
Water	3923.8	---	0.9499	3727.3	---	---	asym. O-H stretch
Complex 1	3333.1	3166.1	---	3029.1	-561.2	-698.2	bound O-H to carbene
	3878.2	3683.9	---	Not observed	-43.4	---	Unbound O-H stretch
Complex 2	3918.8	3722.4	---	Not observed	-4.9	---	asym. O-H stretch

Argon matrix	Calculated frequencies (cm^{-1})	Scaled frequencies (cm^{-1})	Scaling factor	Experimental frequencies (cm^{-1})	Computed shift (cm^{-1})	Experimental shift (cm^{-1})	Mode of assignment
Water	3923.8	---	0.9510	3731.6	---	---	asym. O-H stretch
Complex 1	3333.1	3169.7	---	3019.4	-561.9	-712.2	bound O-H to carbene
	3878.2	3688.1	---	Not observed	-43.5	---	Unbound O-H stretch
Complex 2	3918.8	3726.7	---	Not observed	-4.9	---	asym. O-H stretch

Features corresponding to hydrogen bonded complex of NHC and water were observed in both N_2 as well as Ar matrices. To confirm that these features indeed correspond to hydrogen bonded complex with water, we expect to see features corresponding to hydrogen bonded complex of NHC and some other proton donor solvent (like methanol) in move, so experiments with NHC and methanol system were done in the same manner.

3.2. NHC – Methanol complexes:

3.2.1. Computation

Similarly, the possible complexes which can be formed from 1, 3-dimethylimidazol-2-ylidene and methanol are listed below:

1) Complex 3 (NHC-M1) – Hydroxyl hydrogen of methanol acts as proton donor to the carbene carbon in 1, 3-dimethylimidaol-2-ylidene.
2) Complex 4 (NHC-M2) – Oxygen of methanol acts as proton acceptor to the hydrogen attached to doubly bonded carbon in 1, 3-dimethylimidaol-2-ylidene.

The optimization and frequency calculations were done at R-B3LYP level of theory using 6-311++G (d, p) basis set. The two possible complexes were obtained between 1, 3-dimethylimidazol-2-ylidene and methanol as shown in the **Fig. 24**; namely complex 3 and complex 4. The stabilization energy of these complexes was computed after individually correcting for ZPE and BSSE as shown in **Table 7**. The important structural parameters for these complexes are indicated in **Table 8**. In this case, complex 3 is more stable than complex 4, indicating a global minimum.

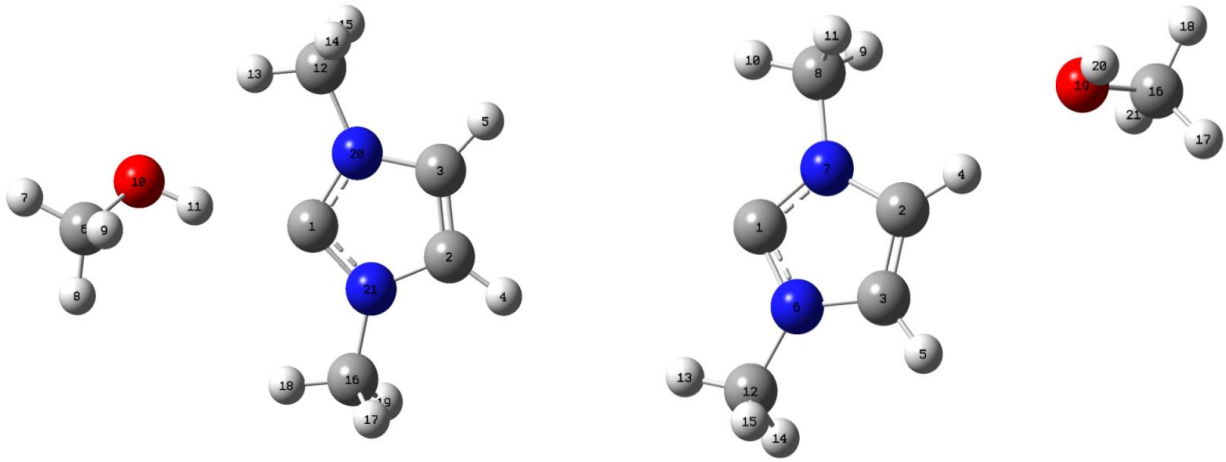

Complex 3 Complex 4

Figure 24: Structures of optimized geometries obtained for the two different complexes of 1, 3-dimethylimidazol-2-ylidene and methanol, computed at R-B3LYP/6-311++G (d, p) level of theory

Table 7: Computed stabilization energies (in kcal mol^{-1}) of 1, 3-dimethylimidazol-2-ylidene and methanol complexes at R-B3LYP/6-311++G (d, p) level of theory

Complex	ΔE_{RAW}	ΔE_{ZPE}	ΔE_{BSSE}
Complex 3 (NHC-M1)	-9.4	-8.2	-8.9
Complex 4 (NHC-M2)	-2.2	-1.6	-1.8

Table 8: Important structural complex parameters, bond lengths (Å), bond angles (°) and dihedral angles (°), of 1, 3-dimethylimidazol-2-ylidene and methanol complexes (as shown in Fig. 24), computed at the R-B3LYP/6-311++G (d,p) level of theory

Complex Parameters	**Complex 3**
r(C1-H11)	1.96
r(H10-O11)	0.99
r(C1-N21)	1.36
r(C2-C3)	1.35
N20-C1-H11	114.71
N21-C1-H11	142.12
C1-H11-O10	165.92
N20-C1-N21	103.00
O10-H11-C1-N21	-179.67
C1-H11-O10-C6	-124.80
H11-C1-N21-C15	-4.92

Complex Parameters	**Complex 4**
r(H4-O19)	2.31
r(H20-O19)	0.96
r(C1-N7)	1.36
r(C2-C3)	1.35
C2-H4-O19	174.27
H4-O19-H20	120.62
H4-O19-C16	123.32
N6-C1-N7	102.15
C2-H4-O19-H20	111.32
C2-H4-O19-C16	-101.29
C3-C2-H4-O19	168.03

AIM analysis

An examination of charge density topology was performed using the atoms-in-molecules (AIM) theory of Bader. (3,-1) bond critical points and (3, +1) ring critical points that could be associated with the complexes were located. The electron density ρ (r_c) and Laplacian (L) of electron density $-\hbar^2\nabla^2/4$ (r_c) for complex 1 and complex 2 were computed for the critical points and the values are shown in **Table 9**. The large value of electron

density for a critical point indicated the strength of non-covalent interaction present at the corresponding sites in the complexes **Fig.25**.

Table 9: AIM calculations for 1, 3-dimethylimidazol-2-ylidene and methanol complexes at R-B3LYP/ 6-311++G (d, p) level of theory

Complex	ρ (r_c) in a.u.	L (r_c) in a.u.
Complex 3 (NHC-M1) **(1)**	0.03468	-0.01636
(2)	0.00757	-0.00628
Complex 4 (NHC-M2)	0.01190	-0.01009

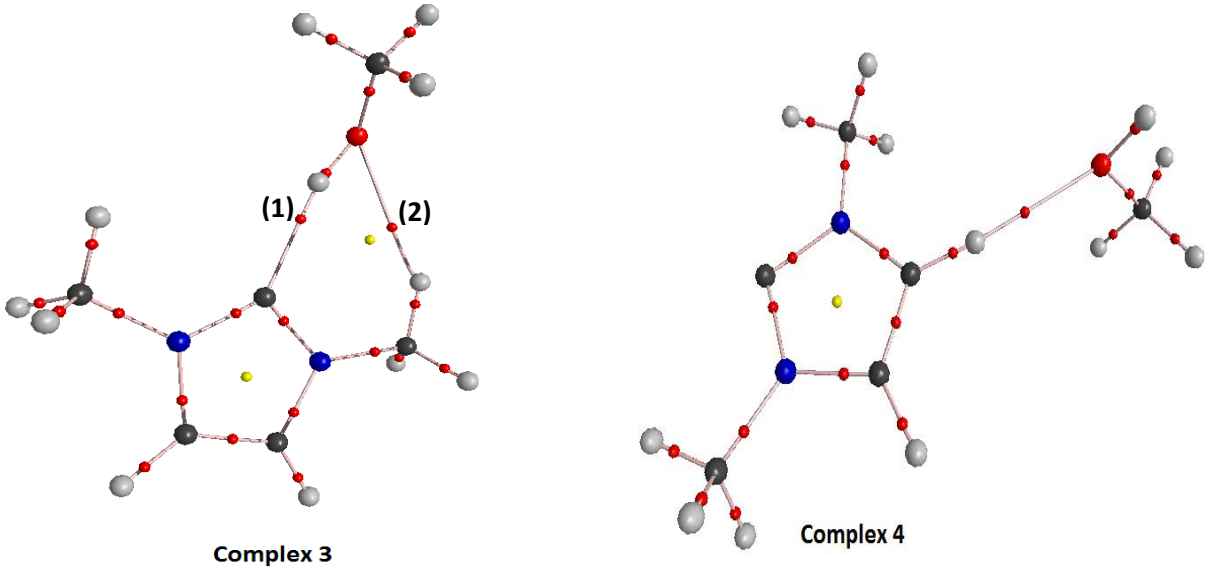

Figure 25: Structures of 1, 3-dimethylimidazol-2-ylidene and methanol complexes showing the bond critical points, computed at R-B3LYP/6-311++G (d, p) level of theory

3.2.2. Experimental and Vibrational analysis:

Fig.26 shows the spectra obtained for 1:1000 concentration of methanol, where peaks at 3664.2 cm^{-1} and 3665.9 cm^{-1}corresponds to O-H stretch of methanol in both N_2 and Ar matrices respectively.

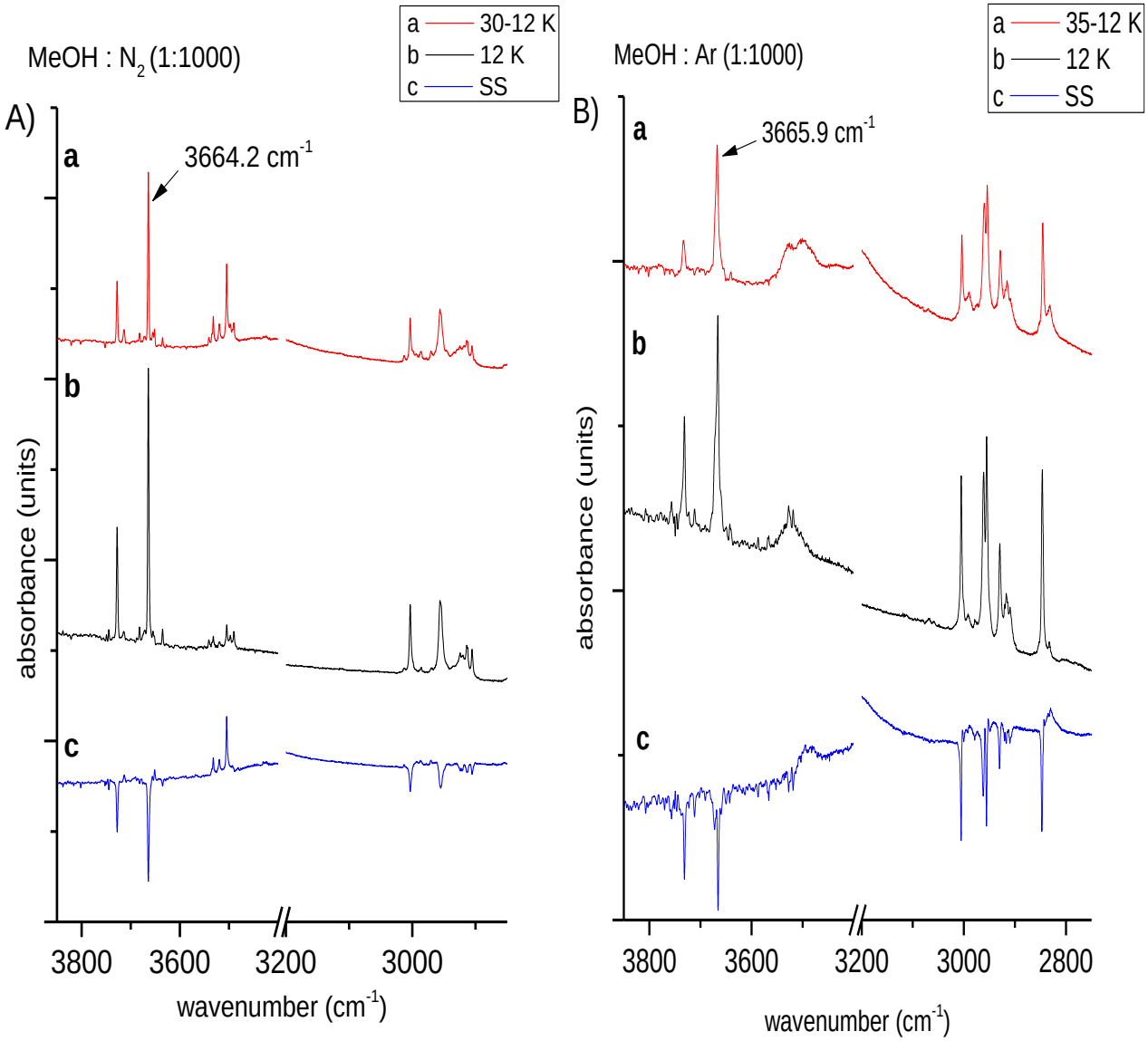

Fig. 26: IR Spectra of Methanol in (A) Nitrogen and (B) Argon matrix: (a) after annealing at 30 K in Nitrogen and at 35 K in Argon matrix (b) at 12 K (c) spectral subtraction (SS)

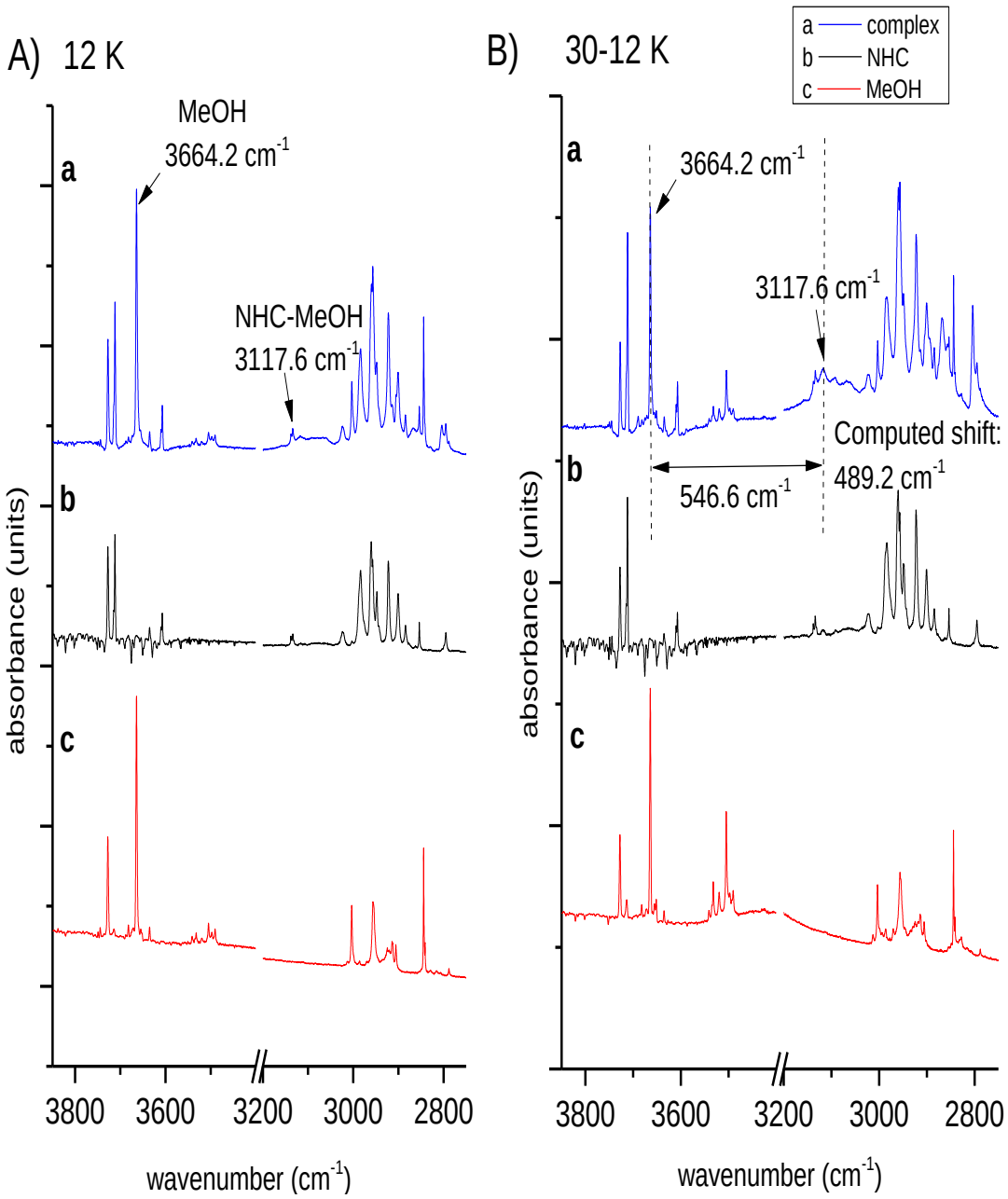

Fig. 27: Comparison of Complex, NHC and MeOH spectra (A) before annealing and (B) after annealing: (a) NHC (120^0C): MeOH: N_2 (1:1000) (b) NHC precursor pyrolyzed at 120^0C (c) MeOH: N_2 (1:1000)

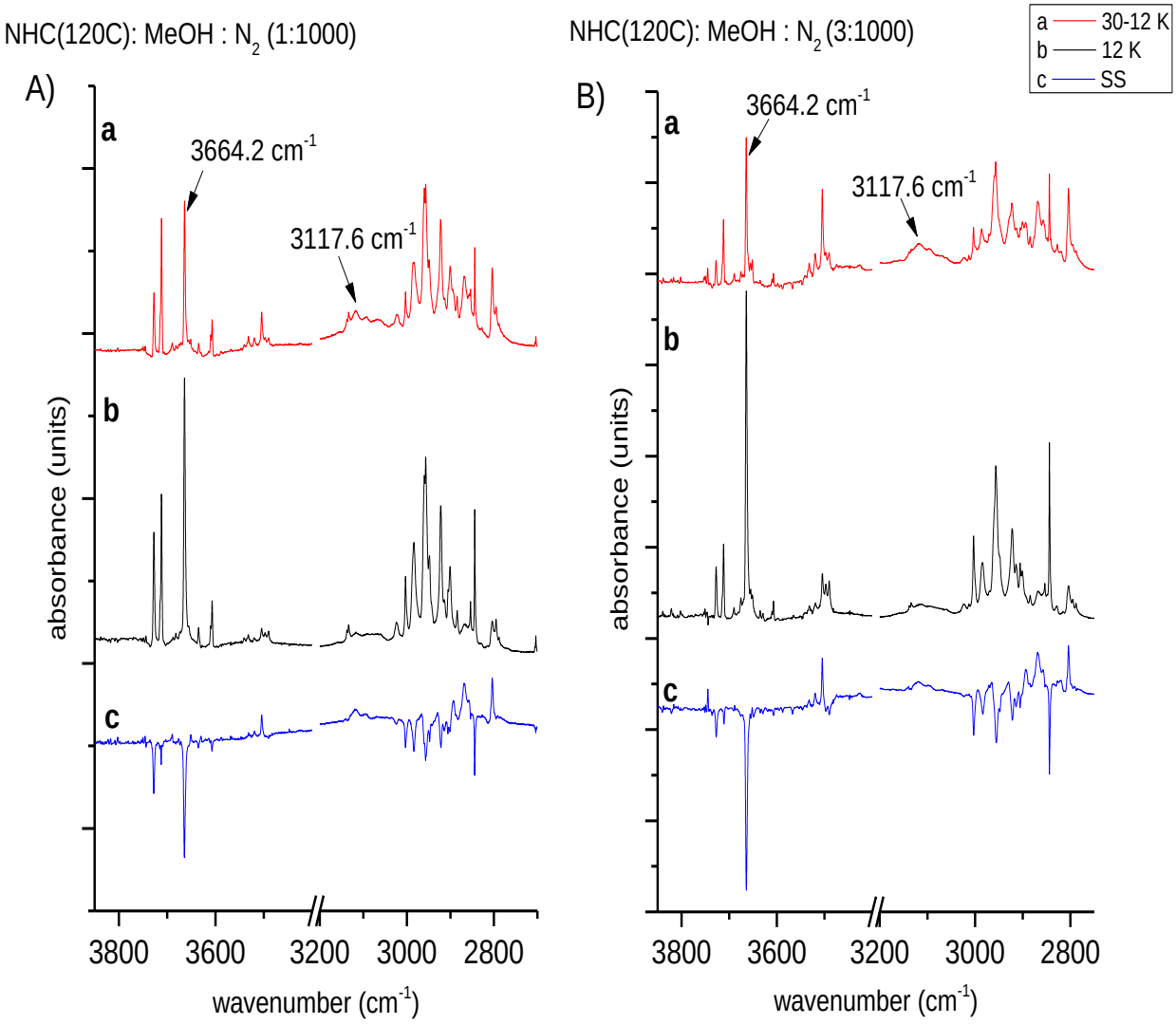

Fig. 28: IR spectra of NHC – MeOH complex showing concentration dependence of MeOH: N_2 {(A) 1:1000 and (B) 3:1000} (a) after annealing at 30 K (b) at 12 K (c) spectral subtraction (SS)

In N_2 matrix, feature corresponding to complex appeared at 3117.6 cm^{-1}. This peak is not observed in NHC and methanol spectra in N_2 matrix (**Fig. 27**) and also increases in intensity after annealing and as the methanol concentration increases three times as shown in the **Fig. 28**. It implies that 3117.6 cm^{-1} peak corresponds to H-bonded complex between NHC and methanol. It is clear from the spectral subtraction that complex feature increases in intensity after annealing.

The possible complexes which can be formed from NHC and methanol are as shown in the **Fig. 24**, namely complex 3 and complex 4. Out of these two complexes,

complex 3 is more stable than that of complex 4 (**Table 7**). Therefore it is likely that complex 3 is observed experimentally. A large red shift of 546.6 cm^{-1} was observed experimentally for the complex in N_2 matrix. It is clear from **Fig. 29** that this experimentally observed red shift (546.6 cm^{-1}) is reasonably good agreement with the computed red shift of complex 3 (489.2 cm^{-1}) than that of complex 4 (0.1 cm^{-1}). Hence, experimentally observed complex feature is assigned as hydrogen bonded feature due to complex 3.

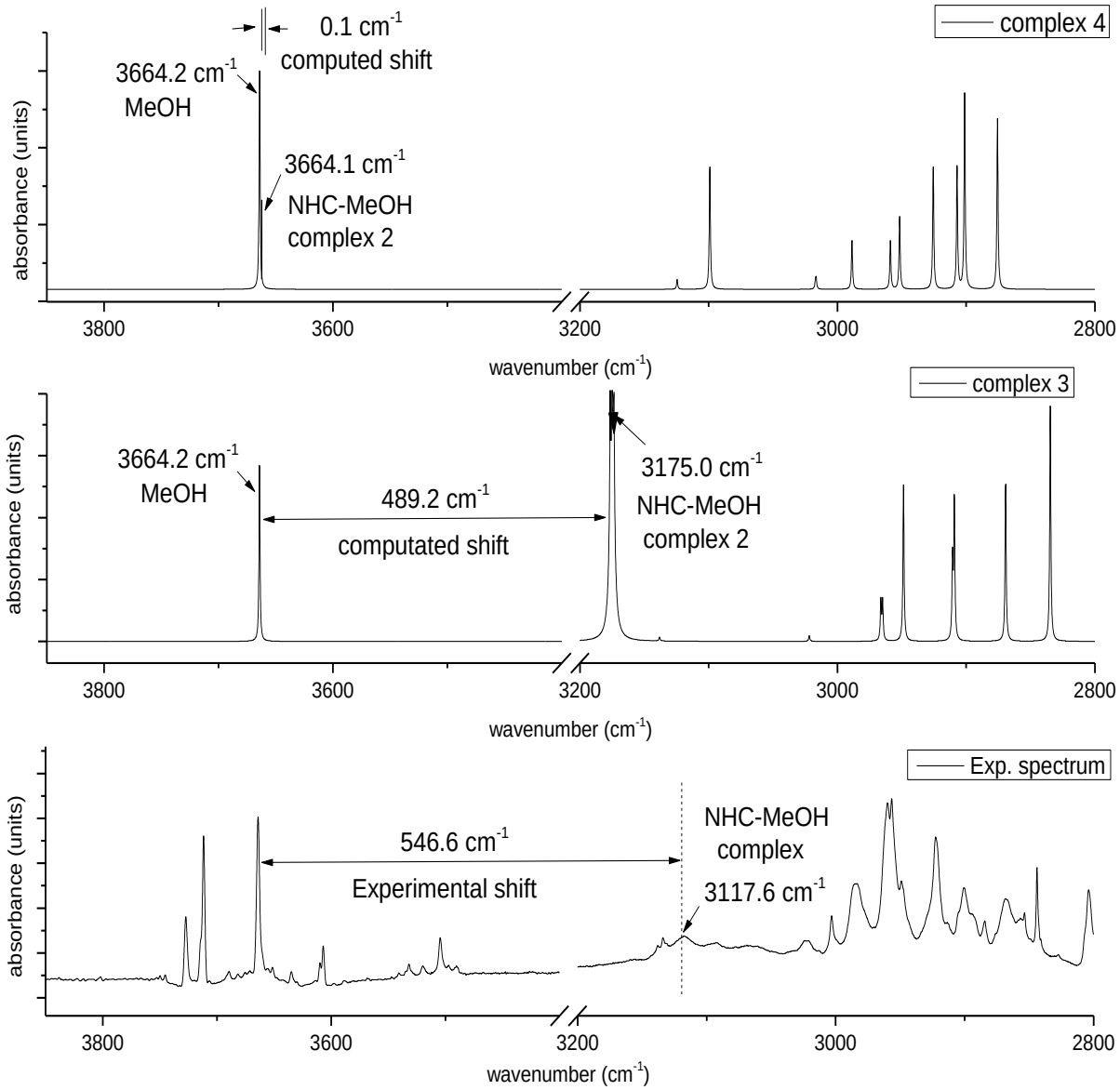

Fig. 29: (a) Computed IR spectrum of NHC-MeOH complex 4 (b) Computed IR spectrum of NHC-MeOH complex 3 (c) Experimental IR spectrum of NHC-MeOH complex trapped in a solid nitrogen matrix

Similar experiments were performed in Ar matrix to ensure that complex feature observed in N_2 matrix is not due to any site effect. In Argon matrix, peak at 3122.3 cm^{-1} can be assigned as complex 3 feature which is not observed in either of NHC and methanol spectra and this feature also increases after annealing as shown in the **Fig. 30** and **Fig. 31**.

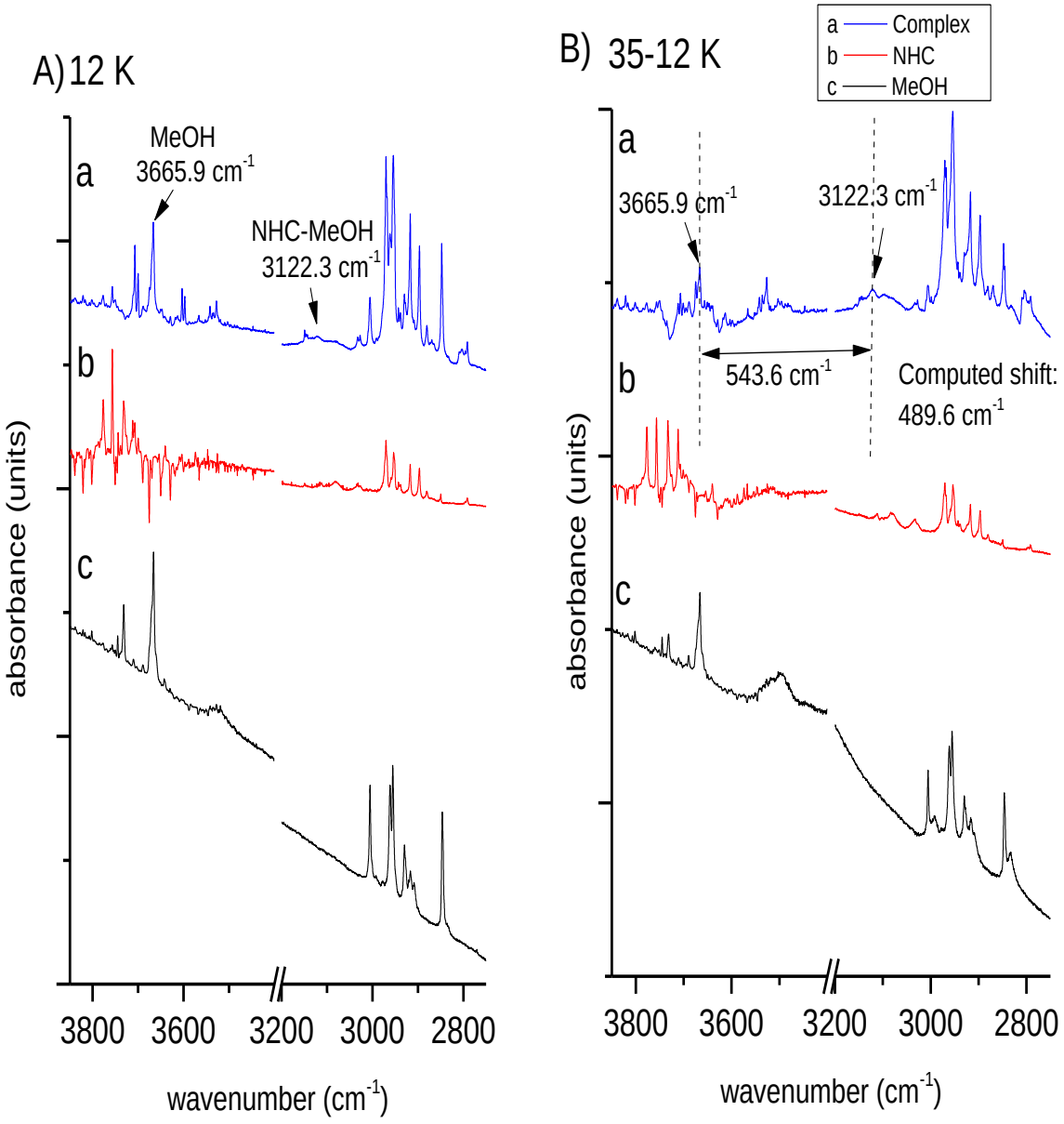

Fig. 30: Comparison of Complex, NHC and MeOH spectra (A) before annealing and (B) after annealing: (a) NHC (80^0C): MeOH: Ar (1:1000) (b) NHC precursor pyrolyzed at 80^0C (c) MeOH: Ar (1:1000)

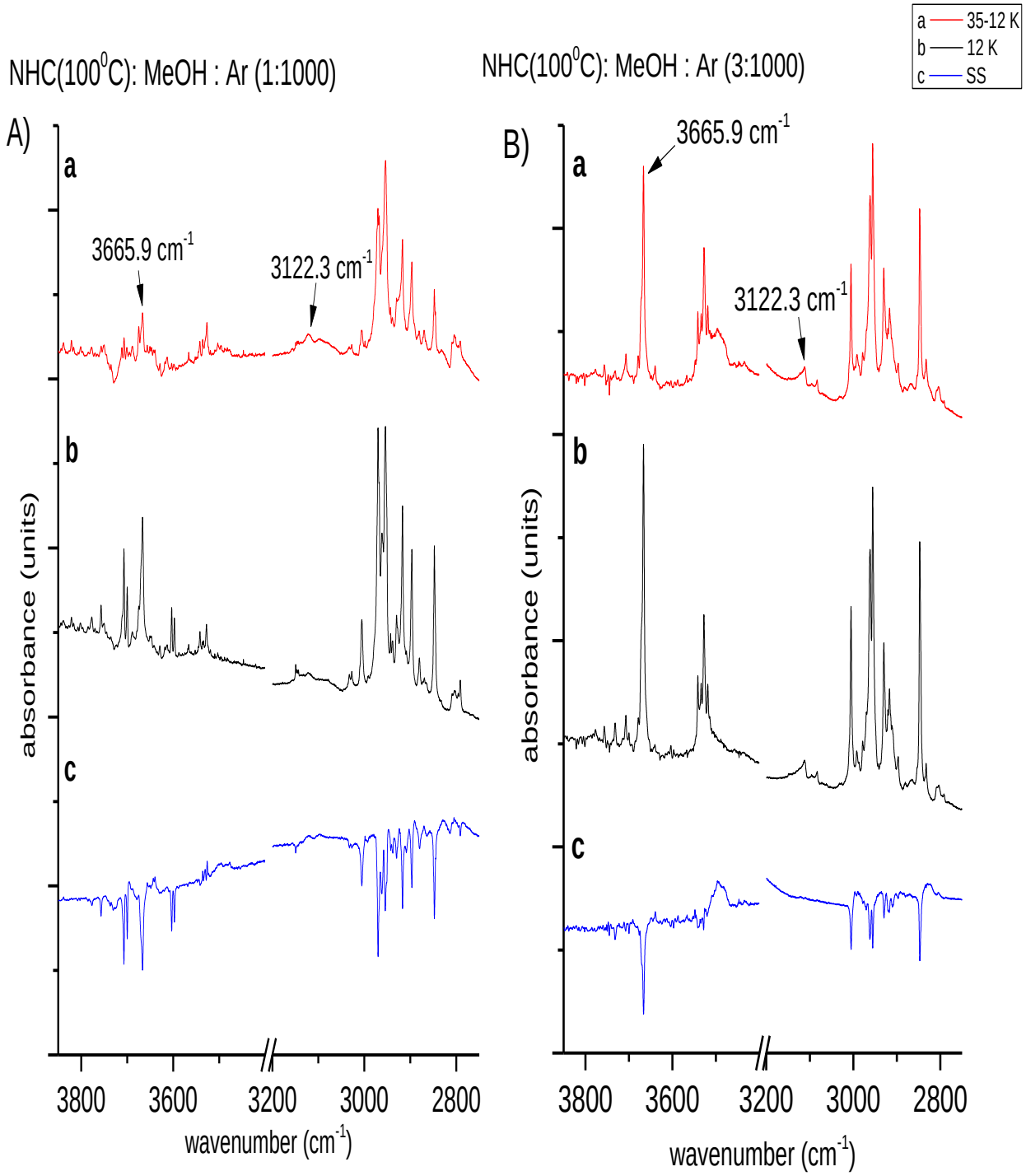

Fig. 31: IR Spectra of NHC – MeOH complex showing concentration dependence of MeOH: Ar {(A) 1:1000 and (B) 3:1000} (a) after annealing at 35 K (b) at 12 K (c) spectral subtraction (SS)

The experimental and computed frequencies for NHC – Methanol complexes are as indicated in **Table 10**. A large red shift of 546.6 cm^{-1} was observed experimentally in case of complex 3 in N_2 matrix, whereas a red shift of 543.6 cm^{-1} was observed for the same in Ar matrix.

Table 10: Experimental and computed frequencies for NHC-MeOH adduct at R-B3LYP/ 6-311++G (d, p) level of theory

Nitrogen matrix	Calculated frequencies (cm^{-1})	Scaled frequencies (cm^{-1})	Scaling factor	Experimental frequencies (cm^{-1})	Computed shift (cm^{-1})	Experimental shift (cm^{-1})	Mode of assignment
Methanol	3845.5	---	0.9528	3664.2	---	---	O-H stretch
Complex 3	3332.3	3175.0	---	3117.6	-489.2	-546.6	bound O-H to carbene
Complex 4	3845.6	3664.1	---	Not observed	-0.1	---	O-H stretch

Argon matrix	Calculated frequencies (cm^{-1})	Scaled frequencies (cm^{-1})	Scaling factor	Experimental frequencies (cm^{-1})	Computed shift (cm^{-1})	Experimental shift (cm^{-1})	Mode of assignment
Methanol	3845.5	---	0.9532	3665.9	---	---	O-H stretch
Complex 3	3332.3	3176.3	---	3122.3	-489.6	-543.6	bound O-H to carbene
Complex 4	3845.6	3665.6	---	Not observed	-0.3	---	O-H stretch

Chapter 4

Conclusions

The thesis provides experimental and computational study of weak interactions between N-heterocyclic carbene and proton donors (water and methanol). The experimental study has been carried out using Matrix Isolation Infrared Spectroscopy. The carboxylate precursor of N-heterocyclic carbene has been pyrolytically decarboxylated and the carbene was trapped in the matrix. It was indicated by copious amount of CO_2 in matrix. Experimental observations have been corroborated by computations. The computational study has been performed by GAUSSIAN 09 programme and the computational analysis has been carried out at B3LYP level of theory using a 6-311++G (d, p) basis set. The BSSE corrected stabilization energies for NHC – H_2O (complex 1) and NHC – MeOH (complex 3) complexes are -9.1 kcal/mol and -8.9 kcal/mol respectively. In these complexes, hydrogen of water/ hydroxyl hydrogen of methanol is forming hydrogen bonded complex with the carbene carbon. Features at 3029.1 cm^{-1} corresponds to hydrogen bonded complex of N-heterocyclic carbene and water with a large red shift of 698.2 cm^{-1} in nitrogen matrix. Whereas, 3019.4 cm^{-1} feature corresponds to the same complex with a large red shift of 712.2 cm^{-1} in argon matrix. To confirm these results, methanol was replaced by water as a proton donor solvent. Feature at 3117.6 cm^{-1} corresponds to hydrogen bonded complex of N-heterocyclic carbene and methanol with red shift of 546.6 cm^{-1} in nitrogen matrix. Whereas, 3122.3 cm^{-1} feature corresponds to the same complex with red shift of 543.6 cm^{-1} in argon matrix. The complex features increase in intensity as water/methanol concentration increases and also increase on annealing.

The ability of N-heterocyclic carbenes to form hydrogen bonded complexes with proton donors provides supportive evidence to proposed mechanism of transesterification reaction in which N-heterocyclic carbene-alcohol hydrogen bonded complex was reported.

Bibliography

1. Schuster, G. B. *Adv. Phys. Org. Chem.* **1986**, *22*, 311.
2. (a) Harrison, J. F. *J. Am. Chem. Soc.* **1971**, *93*, 4112. (b) Bauschlicher, C. W., Jr.; Schaefer, H. F., III; Bagus, P. S. *J. Am.Chem. Soc.* **1977**, *99*, 7106. (c) Harrison, J. F.; Liedtke, C. R.; Liebman, J. F. *J. Am. Chem. Soc.* **1979**, *101*, 7162. (d) Feller, D.; Borden, W. T.; Davidson, E. R. *Chem. Phys. Lett.* **1980**, *71*, 22.
3. Bourissou, D.; Guerret, O.; Gabbaı, F. P.; Bertrand, G. *Chem. Rev.* **2000,** *100*, 39-91.
4. Wanzlick, H. W.; Schonherr, H. J. *Angew. Chem.* **1968,** *80*, 154.
5. Öfele, K. *J. Organomet. Chem.* **1968,** *12*, 42.
6. Arduengo, A. J.; Harlow, R. L.; Kline, M. *J. Am. Chem.* Soc. **1991,** *113,361*.
7. *J. Am. Chem. Soc.***2001**, *123*, 7188-7189, *J. Am. Chem. Soc.***2004**, *126*, 10212-10213, *J. Am. Chem. Soc.***2005**, *127*, 7294-7295.
8. Yamaghuchi.et al. *Organometallics*, **2004**, *23*, 1490-1492, Muniz, K. *Adv. Synth. Catal.* **2004**, *346*, 1425-1428.
9. Mori.et al. *Org. Lett.* **2003**, *5*, 31-33.
10. Furstner.*et al. Org. Lett.* **2002**, *4*, 541-543.
11. Herrmann.*et al. Angw. Chem. Int. Ed*. **1995**, *34*, 2371-2374.
12. Organ.*et al. Org. Lett.* **2005**, *7*, 3805-3807.
13. Ackermann, L. *Org. Lett.* **2005**, *7*, 439-442.
14. Wohler, F. Liebig. *J. Ann. Pharm.* **1832**, *3*, 249-282.
15. Lapworth, A. J. *J. Chem. Soc.* **1903**, *83*, 995-1005.
16. Jousseaume, T.; Wurz, N. E.; Glorius, F. *Angew.chem. Int. Ed.* **2011**,*50*,1410.
17. Kim, S. M.; Jin, M. Y.; Kim, M. J.; Cui, Y.; Kim, Y. S.; Zhang, L.;

Song, C. E.; Ryu, D. H.; Yang, J. W. *Org*. *Biomol.Chem.* **2011**, *2069.*

18. Arnold, B.R.; Bucher, G.; Netto-Ferreira, J.C. *Biradicals, radicals in excited state, carbenes and related species; Springer Verlag*, **1998**.
19. Whittle E.; Dows, D. A.; Pimentel, G. C. *J. Chem. Phys.* **1964**,*22*,1943
20. Norman, I.; Porter, G. *Nature* **1964**, *174*, 508.
21. . Milligan, D. E.; Pimentel, G. C. *J. Chem. Phys.* **1958,** *29*, 1405**.**
22. DeMore, W. B.; Pritchard, H. O.; Davidson, N. *J. Am. Chem. Soc.* **1959**,*81*,5874.
23. Sander, W.W.; Patyk, A.; Bucher, G. Journal of Molecular structure **1990**, *222*, 21-31.
24. Zhang, X.; Anders, V. F., Nandi, S.; Ellison, G.B., *Review of scientific instruments* **2003,** *74*, 3077-3085.
25. George, L.; Sander, W. *Spectrochimica acta Part A* **2004,** *60*, 3225–3232.
26. Hess, K. R.; Samet, C. *Spectroscopy Letters* **2008,** *41*,179–188.
27. Marlies, K. V.; Smets, J.; Nowak, M. J.; Guido, M. *J. Phys. Chem. A* **1997,** *101*, 2397-2413.
28. Rablen P. R.; Lockman J. W.; Jorgensen W. L. *J. Phys. Chem. A* **1998**, *102*, 3782.
29. Sander W.; Costa, P. *Angew. Chem. Int. Ed.* **2014**, *53*, 1-5.
30. Movassaghi M.; Schmidt M. A. *Org. Lett*. **2005**, *7*, 2453-2456.
31. Buckingham, A. D. *Proc. Roy. Soc*. (London) A **1958**, *248*, 169.
32. Voutchkova, A.M.; Feliz, M.; Clot, E.; Eisenstein, O.; Crabtree, R. H. J. Am. Chem. Soc. **2007**, *129*, 12834-12846.
33. Gaussian 09, Revision **A.1**, Frisch, M. J.; Trucks, G. W.; Schlegel, H. B.; Scuseria, G. E.; Robb, M. A.; Cheeseman, J. R.; Scalmani, G.; Barone, V.; Mennucci, B.; Petersson, G. A.; Nakatsuji, H.; Caricato, M.; Li, X.; Hratchian, H. P.; Izmaylov, A. F.; Bloino, J.; Zheng, G.; Sonnenberg, J. L.; Hada, M.; Ehara, M.; Toyota, K.; Fukuda, R.; Hasegawa, J.; Ishida, M.; Nakajima, T.; Honda, Y.; Kitao, O.; Nakai, H.; Vreven, T.; Montgomery, Jr., J. A.; Peralta, J. E.; Ogliaro, F.; Bearpark, M.; Heyd, J. J.; Brothers, E.; Kudin, K. N.; Staroverov, V. N.; Kobayashi, R.; Normand, J.; Raghavachari, K.; Rendell, A.; Burant, J. C.; Iyengar, S. S.; Tomasi, J.; Cossi, M.; Rega, N.; Millam, J. M.; Klene, M.; Knox, J. E.; Cross, J. B.; Bakken, V.; Adamo, C.; Jaramillo, J.; Gomperts, R.; Stratmann, R. E.; Yazyev, O.; Austin, A. J.; Cammi, R.; Pomelli, C.; Ochterski, J. W.; Martin, R. L.; Morokuma, K.; Zakrzewski, V. G.; Voth,

G. A.; Salvador, P.; Dannenberg, J. J.; Dapprich, S.; Daniels, A. D.; Farkas, Ö.; Foresman, J. B.; Ortiz, J. V.; Cioslowski, J.; Fox, D. J. Gaussian, Inc., Wallingford CT, **2009**.

34. Biegle-Koning F.; Bader R. F. W.; Tang W. H. *J. Comput. Chem*. **2000**, *96*, 6796, AIMS 2000.
35. Becke A. D. *Phys. Rev*. A **1989**, *38*, 3098
36. Becke A. D. *J. Chem. Phys*. **1983**, *98*, 5648
37. Scuseria, G. E.; Staroverov, V. N. *Theory and Application of Computational Chemistry*: *the first fourty years*. Elsevier, 669-724
38. Boys, S. F.; Bernadi, F.; *Mol. Phys*. **1970** , *19*, 553
39. Bader R. F. W. *Atoms in Molecules. A Quantum Theory*, Clarendon Press, Oxford, **1994**.